



HHS Public Access

Author manuscript

Immunohorizons. Author manuscript; available in PMC 2022 October 17.

Published in final edited form as:

Immunohorizons. ; 6(4): 253–272. doi:10.4049/immunohorizons.2200018.

LY6S, a New IFN-Inducible Human Member of the Ly6a Subfamily Expressed by Spleen Cells and Associated with Inflammation and Viral Resistance

Moriya Shmerling*, Michael Chalik*, Nechama I. Smorodinsky*, Alan Meeker†, Sujayita Roy†, Orit Sagi-Assif*, Tsipi Meshel*, Artem Danilevsky‡, Noam Shomron‡, Shmuel Levinger*, Bar Nishry*, David Baruchi*, Avital Shargorodsky*, Ravit Ziv*, Avital Sarusi-Portuguez§, Maoz Lahav*, Marcelo Ehrlich*, Bryony Braschi¶, Elspeth Bruford¶, Isaac P. Witz*, Daniel H. Wreschner*

*Shmunis School of Biomedicine and Cancer Research, Tel Aviv University, Ramat Aviv, Israel;

†The Johns Hopkins University School of Medicine, Baltimore, MD;

‡Faculty of Medicine and Edmond J. Safra Center for Bioinformatics, Tel Aviv University, Ramat Aviv, Israel;

§Nancy and Stephen Grand Israel National Center for Personalized Medicine, Weizmann Institute of Science, Rehovot, Israel;

¶HUGO Gene Nomenclature Committee, European Molecular Biology Laboratory, European Bioinformatics Institute, Wellcome Genome Campus, Hinxton, Cambridgeshire, United Kingdom;

||Department of Haematology, University of Cambridge School of Clinical Medicine, Cambridge Biomedical Campus, Cambridge, United Kingdom

Abstract

Syntenic genomic loci on human chromosome 8 and mouse chromosome 15 (mChr15) code for LY6/Ly6 (lymphocyte Ag 6) family proteins. The 23 murine *Ly6* family genes include eight genes that are flanked by the murine *Ly6e* and *Ly6l* genes and form an Ly6 subgroup referred

This article is distributed under the terms of the [CC BY-NC-ND 4.0 Unported license](https://creativecommons.org/licenses/by-nc-nd/4.0/).

Address correspondence and reprint requests to: Prof. Daniel H. Wreschner and Prof. Isaac P. Witz, Shmunis School of Biomedicine and Cancer Research, Tel Aviv University, Ramat Aviv, Israel. dwreschner@gmail.com (D.H.W.) and isaacw@tauex.tau.ac.il (I.P.W.).

Discovery of LY6S: D.H.W., M.S., and M.C.; immunofluorescent and immunohistochemical studies: A.M., S.R., and M.C.; analyses of RNA sequencing datasets: N.S., A.D., A.S.-P., and D.H.W.; anti-LY6S-iso1 mAbs: D.H.W., O.S.-A., R.Z., and N.I.S.; cell transfectants expressing LY6S proteins: T.M., O.S.-A., S.L., B.N., D.B., A.S., R.Z., and D.H.W.; viral resistance of LY6S-iso1-expressing cells: M.L. and M.E.; phylogenetic analyses and gene annotation: E.B., B.B., and D.H.W.; writing – original draft: D.H.W., E.B., B.B., N.S., and A.D.; writing – review and editing: D.H.W., E.B., M.E., and I.P.W.; funding acquisition: I.P.W. and D.H.W.; project administration: D.H.W. and I.P.W.; supervision: D.H.W. and I.P.W.

DISCLOSURES

The authors have no financial conflicts of interest.

The RNA-seq data presented in this article have been submitted to the Gene Expression Omnibus (GEO) database under accession numbers GSE188924 (<https://www.ncbi.nlm.nih.gov/geo/query/acc.cgi?acc=GSE188924>) and GSE159456 (<https://www.ncbi.nlm.nih.gov/geo/query/acc.cgi?acc=GSE159456>).

The online version of this article contains supplemental material.

Supplementary Material <http://www.immunohorizons.org/content/suppl/2022/04/19/immunohorizons.2200018.DCSupplemental>

to in this article as the Ly6a subfamily gene cluster. *Ly6a*, also known as *Stem Cell Ag-1* and *T cell-activating protein*, is a member of the Ly6a subfamily gene cluster. No *LY6* genes have been annotated within the syntenic *LY6E* to *LY6L* human locus. We report in this article on *LY6S*, a solitary human *LY6* gene that is syntenic with the murine Ly6a subfamily gene cluster, and with which it shares a common ancestry. *LY6S* codes for the IFN-inducible GPI-linked LY6S-iso1 protein that contains only 9 of the 10 consensus LY6 cysteine residues and is most highly expressed in a nonclassical spleen cell population. Its expression leads to distinct shifts in patterns of gene expression, particularly of genes coding for inflammatory and immune response proteins, and LY6S-iso1-expressing cells show increased resistance to viral infection. Our findings reveal the presence of a previously unannotated human IFN-stimulated gene, *LY6S*, which has a 1:8 ortholog relationship with the genes of the Ly6a subfamily gene cluster, is most highly expressed in spleen cells of a nonclassical cell lineage, and whose expression induces viral resistance and is associated with an inflammatory phenotype and with the activation of genes that regulate immune responses.

INTRODUCTION

The human genome contains at least 48 Lymphocyte Ag 6 (LY6) genes and the mouse genome at least 61 Ly6 genes, all coding for three-fingered proteins (TFPs) that contain a signature pattern of 10 cysteine residues, resulting in a distinctive disulfide bonding pattern. They contain a domain found in the urokinase-type plasminogen activator receptor protein (uPAR, encoded by *PLAUR*) and are also referred to as LY6/uPAR or LU proteins. These proteins locate extracellularly either linked to the cell membrane via a GPI anchor, as transmembrane proteins, or as fully secreted proteins as seen, for example, in the PATE proteins (1). The transmembrane proteins include the receptors for proteins belonging to the TGF- β family, such as BMP2 and activin (2). Only a few of the TFP/LY6/uPAR proteins have known functions, with the most well characterized being CD59 (3, 4), uPAR/PLAUR (5), and GPIHBP1 (6). A common theme for these proteins is that the LY6 domain mediates interactions with other proteins. The variety of functions both known and postulated for the LY6 family proteins suggests that nature has usurped the skeleton scaffold of the TFP fold to execute a large number of diverse activities (7–10).

Mouse chromosome 15 (mChr15) harbors a locus replete with 23 *Ly6* family genes (Fig. 1a), most of which code for Ly6 proteins linked to the cell surface by a GPI anchor. One of the most widely investigated *Ly6* genes is *Ly6a*, which is located within the chromosome 15 locus (11) and codes for an IFN-inducible GPI-linked protein, also known as T cell-Activating Protein and stem cell Ag-1. *Ly6a* is upregulated by IFNs and is implicated in the activation of T cells, as well as in inflammatory and immune-related processes. Similarly, the murine genes *Ly6c* and *Ly6g*, which genomically cocluster with *Ly6a*, are used extensively to analyze cells of the myeloid lineage, especially of the mouse spleen (e.g., Refs. 12–14), and *Ly6c* expression is used as a marker for murine blood monocytes (15, 16). Furthermore, the murine Ly6 genes *Ly6a*, *Ly6c*, and *Ly6g* are inducible by IFNs and code for proteins that are markedly upregulated in inflammatory processes and immune-related diseases (17–19). Despite the hundreds of publications on each of these three murine genes, many focusing on their role in inflammation, their precise functions have yet to be

elucidated. It is all the more so surprising that no human homolog(s) to this murine Ly6a, Ly6c, and Ly6g gene subfamily has been previously identified.

We report in this article the identification of a new human LY6 gene designated LY6S by the HUGO Gene Nomenclature Committee (20) that codes for a LY6 protein that phylogenetic analyses indicate has an orthologous relationship with the murine Ly6a subfamily cluster. Human LY6S codes for a membrane-linked protein that is most highly expressed in the human spleen by a nonclassical human spleen cell and is associated with the regulation of cell growth, inflammatory and immune-related responses, and resistance to infection by certain viruses.

MATERIALS AND METHODS

Reagents and Abs

All chemicals and reagents were obtained from Sigma (St. Louis, MO), unless otherwise specified. Secondary Abs used in cell counterstaining or in immunohistochemical development were obtained from Jackson ImmunoResearch Laboratories (Bar Harbor, ME).

Immunization of mice and generation of hybridomas

Mice were immunized with five consecutive intradermal immunizations spaced at 21-d intervals, with peptide E, derived from the amino acid sequence of LY6S-iso1 (see Fig. 6a), covalently conjugated to Keyhole Limpet Hemocyanin. The mice were purchased from Harlan Laboratories Limited (Israel) and were housed and maintained in laminar flow cabinets under specific pathogen-free conditions in the animal quarters of Tel Aviv University. All work was performed in accordance with current regulations and standards of the Tel Aviv University Institutional Animal Care and Use Committee. The initial immunization was done with Freund's adjuvant, and the following four peptide E covalently conjugated to Keyhole Limpet Hemocyanin boost immunizations together with IFA. Hybridomas were prepared by fusion of nonsecreting myeloma cells with immune splenocytes and screened by ELISA assay (see later).

ELISA for determining binding of anti-LY6S-peptide E mAbs to LY6-iso1 protein

ELISA Immunoassay plates (CoStar) were coated with recombinant hFc-LY6-iso1 protein, produced and secreted by HEK 293 cells stably transfected with and secreting hFc-LY6S-iso1 protein (see later Expression of hFc-LY6S fusion protein section). Spent culture media from the initial hybridomas were then applied to the wells. After incubation, samples were removed and the wells were washed with PBS/Tween. Detection of bound Abs was done with HRP-conjugated anti-mouse Ab.

Expression of hFc-LY6S fusion protein

The hFc-LY6S fusion protein was generated by inserting DNA coding for this protein into the pcDNA3.1 expression vector using standard molecular biology techniques. The make-up of this insert, the amino acid sequence of the resultant fusion protein and the DNA sequence of the insert, are shown in Supplemental Fig. 1.

Sequence determination of SCA5E12 anti-LY6-iso1 mAbs

RNA was isolated from the SCA5E12 hybridoma (anti-LY6-iso1 mAb) with TRIzol Reagent 1, according to a technical manual for the reagent (Ambion, Foster City, CA). The sequence of the SCA5E12 Ab was determined as follows: cDNA was generated by reverse transcription of total RNA with the use of universal or isotype-specific antisense primers, according to the technical manual for PrimeScript First Strand cDNA Synthesis Kit (Takara Bio, Mountain View, CA). Amplification of V_H and V_L Ab fragments was carried out according to the standard operating procedure (GenScript), which involves rapid amplification of cDNA ends, followed by separate cloning into a standard cloning vector. Clones with inserts of the correct sizes were sequenced by colony PCR, and at least five colonies with such inserts were sequenced for each fragment, with the consensus sequence derived by alignment of the different clones.

Immunohistochemistry

Chromogenic immunolabeling for SCA5E12 was performed on formalin-fixed, paraffin-embedded human tissue sections. Briefly, after dewaxing and rehydration, slides were immersed in 1% Tween 20, then heat-induced Ag retrieval was performed in a preheated steamer using Ag Unmasking Buffer (catalog #H-3300; Vector Labs) for 25 min. Slides were rinsed in PBST and endogenous peroxidase, phosphatase was blocked (catalog #S2003; Dako), and sections were then incubated with primary SCA5E12 mouse mAb (1:50 dilution) for 45 min at room temperature. For staining in the presence of competing peptides, primary Ab was diluted 1:10 in the peptide solution directly. The primary Abs were detected by 30-min incubation with HRP-labeled anti-mouse secondary Ab (catalog #PV6114; Leica Microsystems) followed by detection with 3,3'-diaminobenzidine (catalog #D4293; Sigma-Aldrich), counterstaining with Mayer's hematoxylin, dehydration, and mounting.

Immunofluorescence

Dual OPAL immunofluorescent labeling with SCA5E12 and anti-CD45 Abs (catalog #145M-94; Cell Marque/Sigma-Aldrich) was performed on formalin-fixed, paraffin-embedded tissue sections following the manufacturer's instructions (NEL810001KT; Akoya Biosciences, Menlo Park, CA). Briefly, after standard dewaxing and rehydration, slides were immersed in Ag Unmasking Buffer (H-3300 Vector Laboratories; Burlingame, CA) in a plastic chamber and retrieved in a microwave, which is also the subsequent Ab stripping step for sequential multiplex staining. Endogenous peroxidase and phosphatase were blocked (catalog #S2003; Dako), and sections were then incubated sequentially with each primary Ab (1:80 dilution for SCA5E12 and specific dilutions for the other primaries as listed later) for 45 min at room temperature with Ab stripping step performed in between. Slides were incubated with differently labeled anti-Mouse IgG (PV6114; Leica, Wetzlar, Germany) or anti-rabbit IgG (PV6119; Leica) secondary Abs, as appropriate, for 30 min. Fluorescent dyes OPAL 520 (for each of the Abs listed later) and OPAL 690 (for SCA5E12) were diluted in OPAL amplification buffer, and slides were stained for 10 min. Slides were counterstained with DAPI working solution for 10 min, washed, and mounted with ProLong Gold.

The specific primary Abs used for dual immunofluorescence with the SCA5E12 Ab were anti-CD4 (ab133616, 1:200, rabbit; Abcam), anti-CD8 (m0814, 1:100, mouse; Dako),

anti-CD11b (ab133357, 1:8000, rabbit; Abcam), anti-CD11c (ab52632, 1:100, rabbit; Abcam), anti-CD19 (catalog #119M-14, 1:50, mouse; Cell Marque/Sigma-Aldrich), anti-CD20 (0755, 1:100, mouse; Dako), anti-CD31 (RB-10333-P, 1:50, rabbit; Thermo Fisher Scientific), anti-CD34 (catalog #134M-14, 1:75, mouse; Cell Marque/Sigma-Aldrich), anti-CD45 (catalog #145M-94, 1:100, mouse; Cell Marque/Sigma-Aldrich), anti-CD68 (m0814, 1:250, mouse; Dako), anti-CD117 (c-Kit; A450229-2, 1:400, rabbit; Dako), *Pan*-cytokeratin AE1/AE3 (ab961, 1:10, mouse; Abcam), and anti-FOXP3 (12653S, 1:50, rabbit; Cell Signaling Technologies).

Samples used for immunohistochemical stainings were procured from the Biomax tissue bank, with all required ethical approvals therein, as stated at <http://biomax.us>: “All tissue is collected under the highest ethical standards with the donor being informed completely and with their consent. We make sure we follow standard medical care and protect the donors’ privacy. All human tissues are collected under HIPPA approved protocols.”

Generation of pQCXIP plasmids coding for LY6S proteins and generation of stable cell infectants expressing the LY6S proteins

Total RNA was extracted from human melanoma M12-CB2 cells that were treated with IFN- γ for 48 h using the EZ-RNA Total RNA Isolation Kit (Biological Industries, Kibbutz Beit-Haemek, Israel), followed by cDNA synthesis with qScript cDNA Synthesis Kit (Quantabio). The overexpression construct of human LY6 was created by PCR amplification of cDNA by Phusion High-Fidelity DNA polymerase (Thermo Fisher Scientific), using the following primers LY-6S-Pac1-S-5’-GGAACGTTAATTAACGC-TGAAGTTTGTCTGTGCACTA-3’, LY6S-EcoR1-AS-5’-AGAGAG-GAATTCCTCAAGCAGCTGGTGACGCACAG-3’. The generated fragment was digested with Pac1 and EcoR1 and ligated into the corresponding sites of pQCXIP vector (Clontech Laboratories, Mountain View, CA). PCR products of LY6S were sequenced. Cells were infected to stably express LY6S-pQCXIP retroviral vector (Clontech Laboratories) as described previously (21).

Vesicular stomatitis virus infection

M12, YDFR, or U87 cells were infected with vesicular stomatitis virus (VSV)-New Jersey (a gift of Prof. M. Kotler, Hebrew University) at multiplicities of infection of 0.5, 0.15, or 0.05 for 24 or 48 h. Titer of inoculum or of spent medium of infected cells was measured by plaque assay on Vero cells: sequential 10-fold dilutions in DMEM, and 125,000 cells per well of a 12-well plate. Overlay was with 0.6% methylcellulose. Detection was by crystal violet staining.

Flow cytometry

Ag expression was determined using Flow cytometer S100EXi (Stratedigm, San Jose, CA) with CellCapTure software and FlowJo v10. Dead cells were gated out from the analysis.

Phylogenetic tree analysis

Sequences were aligned by using the Muscle Multiple Sequence alignment software (PMID: 30976793) available through an online server at the EBI (<https://www.ebi.ac.uk/Tools/msa/>

muscle). AliView (PMID: 25095880) was used to view and edit the initial alignment of 303 columns. The alignment was edited to remove indel regions of ambiguous alignment, and columns with <20% gaps were retained, providing a final alignment of 113 aa.

ProtTest-3.4.2 (22) was used to determine the best fit evolutionary model for this maximum likelihood analysis. The RAxML-NG (PMID: 31070718) blackbox server (<https://raxml-ng.vital-it.ch/#/>) was used to perform a maximum likelihood analysis (JTT+G4m substitution model, stationary base frequencies taken from the model, with the proportion of invariant sites box selected, and four γ rate categories to model the among-site rate heterogeneity), with automatic bootstopping of the bootstrapping procedure, as implemented in RAxML. Trees were visualized and edited with FigTree v1.4.3 software (<http://tree.bio.ed.ac.uk/software/figtree/>).

mRNA sequencing

Libraries were prepared by the Crown Institute for Genomics (G-INCPM, Weizmann Institute of Science) using an in-house poly(A)-based RNA sequencing (RNA-seq) protocol (INCPM-mRNA-seq). Briefly, the poly(A) fraction (mRNA) was purified from 500 ng of total input RNA followed by fragmentation and the generation of double-stranded cDNA. After Agencourt Ampure XP beads cleanup (Beckman Coulter), end repair, A base addition, adapter ligation, and PCR amplification steps were performed. Libraries were quantified by Qubit (Thermo Fisher Scientific) and TapeStation (Agilent). Sequencing was done on a Nextseq 75 cycles high-output kit, allocating 20M reads per sample (Illumina; single-read sequencing). The RNA-seq data, GEO accession number GSE188924, have been uploaded to the GEO database. This SuperSeries record provides access to all of the data relating to both the control human cells (U87 glioblastoma, M12 melanoma, and YDFR melanoma cells) and their counterparts expressing the LY6S-iso1 protein. To review, it can be accessed at: <https://www.ncbi.nlm.nih.gov/geo/query/acc.cgi?acc=GSE188924>. The Paired End (PE) True Stranded RNA-seq data, GEO accession number GSE159456, have also been uploaded to the GEO database (<https://www.ncbi.nlm.nih.gov/geo/query/acc.cgi?acc=GSE159456>).

Data analysis for RNA-seq

Poly-A/T stretches and Illumina adapters were trimmed from the reads by using cutadapt; reads <30 bp were discarded. Reads for each sample were aligned independently to human reference genome GRCh38 with STAR (23) and supplied with gene annotations downloaded from Ensembl (and with the EndToEnd option). Counting proceeded over genes annotated in Ensembl release 92 using the htseq-count (with stranded = "reverse" option for the PE) (24). Only uniquely mapped reads were used to determine the number of reads falling into each gene (intersection-strict mode). Differential analysis was performed with the DESeq2 package (25), with the betaPrior, cooksCutoff, and independentFiltering parameters set to False. Raw *p* values were adjusted for multiple testing by using the Benjamini and Hochberg procedure. Differentially expressed genes were determined by an adjusted *p* value of <0.05, absolute fold changes > 2, and max raw counts > 30. Functional analysis of DE genes was performed with Ingenuity Pathway Analysis (IPA; QIAGEN; <https://www.qiagenbioinformatics.com/products/ingenuity-pathway-analysis>), together with Martin's (26) method and also methods detailed elsewhere (23–25, 27).

RESULTS

Analysis of mChr15 and human chromosome 8 Ly6/LY6 loci reveals a new human LY6 gene syntenic with Ly6a

Murine *Ly6a* resides on mChr15 in a 900-kb genomic locus replete with other genes coding for Ly6 family proteins (Fig. 1a). The syntenic human locus on chromosome 8 is also rich in LY6 genes, yet at ~540 kb is considerably smaller than the corresponding mouse locus and contains far fewer LY6 family genes (Fig. 1b). The murine subregion containing *Ly6a* is demarcated by the *Ly6e* and *Ly6l* genes, spans ~500 kb, and contains eight Ly6 genes. In contrast, the human *LY6E* and *LY6L* genes (Fig. 1b) span a region of ~60 kb within which no annotated LY6 genes reside.

A phylogenetic tree analysis of the human chromosome 8 (hChr8) and mChr5 LY6 loci (Fig. 1e) shows that the eight Ly6 family genes located within the 500-kb subregion group together in a clade with high bootstrap support and are more distantly related to the Ly6 genes located outside of the *Ly6e* to *Ly6l* locus. Cumulatively, this indicates that the eight genes within the *Ly6e* to *Ly6l* locus form a Ly6 family subgroup, referred to in this study as the Ly6a subfamily. In contrast with the murine Ly6a subfamily locus, the corresponding syntenic human region also flanked by *LY6E* and *LY6L* is only ~60 kb (Fig. 1b) and contains no annotated human LY6 genes.

Because the mouse *Ly6a* gene lies downstream of *Ly6e*, within the genomic neighborhood demarcated by the *Ly6e* and *Ly6l* genes, and because *LY6L* is predicted to be the human ortholog of *Ly6l* by multiple orthology resources (see the HUGO Gene Nomenclature Committee HCOP tool: https://www.genenames.org/data/gene-symbol-report/#!/hgnc_id/HGNC:52284), we expected that if a human ortholog of *Ly6a* were to exist, then it too should reside within the human syntenic segment bordered by *LY6E* and *LY6L*, which spans only ~60 kb (see Fig. 1b). No annotated human LY6 genes appear in this region. Yet, GenScan predicts a gene (chr8_73.103, here designated as LY6S; Fig. 1c, and see later) that codes for an LY6 family protein that shows a high level of sequence homology to the mouse Ly6a protein. Furthermore, the TransMap cross-species alignment algorithm (28, 29) that maps genes and related annotations in one species versus another by using synteny-filtered pairwise genome alignments to determine the most likely ortholog, maps *Ly6a* at the same position as the GenScan predicted human LY6 gene.

Experimental confirmation for LY6S mRNAs

Neither expressed sequence tags nor any other experimental evidence supports the GenScan chr8_73.103 (LY6S) gene. Notably, transcription of the LY6S gene (Fig. 1c) is in the opposite direction to that of a known gene, *C8orf31*, that is transcribed from the complementary strand and has extensive exon overlap with exons from the human LY6S gene (Fig. 2a, 2b). Oligonucleotide primers were identified that are specific solely for LY6S and do not overlap with *C8orf31* (see Fig. 2c and Supplemental Table I). RT-PCR analyses with these primers revealed a particularly prominent RT-PCR product in the human spleen (Fig. 2di, 2dii), which showed the highest expression (Fig. 2di, 2dii, 2e). Of all fetal tissues, spleen was also the highest *LY6S* expresser (inset, Fig. 2e). In contrast with

its high expression in the lymphoid-rich spleen, *LY6S* expression was not detected in peripheral blood leukocytes or in bone marrow (Fig. 2di, compare lanes 1 and 8 with lane 18 [bone marrow, leukocytes and spleen, respectively], Fig. 2e). In addition to spleen, *LY6S* expression was detected in brain tissue (Fig. 2di, lane 2, and at higher contrast in Fig. 2di', lane 2). In line with these results, increasing the number of PCR cycles to 40 showed, as expected, highest expression in spleen followed by testis (Fig. 2h, lanes 14 and 16, respectively). Significant expression was also detected in the parietal lobe of the brain and in the spinal cord, and lower levels in the thalamus and temporal lobe (Fig. 2h, lanes 8, 13, 17, and 15, respectively). Use of a different set of primers, the F8 and R12 forward and reverse primers (Supplemental Table I), confirmed these results, and highest expression was again observed in the spleen, with significant expression observed in the parietal lobe and corpus callosum, and with lower levels in the cerebral cortex and temporal lobe (Fig. 2i, lanes 1, 8, 9, 4, and 7, respectively). With both sets of primers, the F7 and R10 and F8 and R12 pairs, the sizes of the observed RT-PCR products correlated precisely to those expected for expression of *LY6S* (Fig. 2di, 2di', 2dii, 2h for the F7 and R10 primer pair; Fig. 2f, 2g [see later], 2h-j for the F8 and R12 primer pair).

Whereas RT-PCR analyses revealed significant *LY6S* expression in human spleen tissue, similar analyses performed on a number of different human cell lines failed to detect *LY6S* expression. *Ly6a*, as well as other mouse *Ly6* genes, such as *Ly6c1*, are highly induced by IFNs, and human *LY6E* located upstream to *LY6S* is induced by both type I (α/β) and type II (γ) IFNs. We postulated that *LY6S* may also be IFN inducible. A perfect IFN-stimulated response element positioned ~500 bp upstream to the *LY6S* gene appears as TTCCTGTGAAATGGAAATTCAGGA (underlined sequence is identical to the IFN-stimulated response element conferring IFN inducibility on one of the human IFN- α genes) and conforms to the tandem GAAANNGAAA element that appears in most type I IFN-stimulated genes (ISGs). This stretch of 24 nt also contains the palindromic consensus sequence TTCN₂₋₄GAA (TTCCTGTGAA) that conforms to the consensus IFN- γ activation site. We thus assessed *LY6S* expression in different human cell lines, either untreated or exposed to IFN- α , IFN- β , or IFN- γ , and compared *LY6S* expression with that of *LY6E*. Because of the number of PCR cycles used in this experiment (36 cycles), *LY6E* expression was observed at high levels in all cell lines irrespective of IFN treatment (Fig. 2f, upper panel). In the absence of cytokine treatment, none of the human cell lines expressed significant levels of *LY6S*, as shown for the M12CB3 and YCB3 melanoma cells (Fig. 2g, lane 1, and Fig. 2ji, 2jii, lane 1) and for the MCF7 breast cancer cells (Fig. 2jiii, lane 1). Treatment with IFN- β induced marked *LY6S* expression in several cell lines, including U87 glioblastoma cells (Fig. 2f, lanes 8 and 12), MCF7 breast cancer cells (Fig. 2f, lane 18, and Fig. 2jiii, lane 2), and HEY ovarian cancer cells (Fig. 2f, lane 17). IFN treatment induced *LY6S* expression in M12CB3 melanoma cells (Fig. 2g, lanes 2-4, for IFN- α , IFN- β , and IFN- γ , respectively, and Fig. 2ji, lane 2) and in YCB3 melanoma cells (Fig. 2jii, lane 2). Notably, *LY6S* isoforms 1 and 2 (see later for description of isoforms 1 and 2) were induced to varying extents by the different IFNs (Fig. 2g, compare lanes 2-4).

TOPO cloning and nucleotide sequencing of the *LY6S* RT-PCR product(s) obtained with human spleen cDNA (see Fig. 2di, lane 18) revealed three inferred protein isoforms (see Fig. 3 and Supplemental Fig. 2 for detailed information on *LY6S*-iso1 and iso2) corresponding to

(1) a LY6S protein, which received a perfect GPI score from the GPI anchor predictor tool PredGPI, indicating that it is a GPI-linked membrane-bound protein (isoform 1, designated LY6S-iso1, in three of eight sequenced TOPO clones; Fig. 3a, isoform 1); (2) a C-terminally truncated LY6S protein, likely to be secreted from the cell that retains both exon 1 (signal peptide [SP]) and exon 2 coding sequences but uses an alternative splice donor site toward the 3' end of exon 2 (isoform 2, designated LY6S-iso2, for four of eight sequenced TOPO clones; Fig. 3b, isoform 2); and (3) a protein that retains the exon 1 SP, but by use of an alternative splice acceptor site produces a frameshifted protein C-terminal to the SP, which is also likely to be secreted from the cell (isoform 3, for one of eight sequenced TOPO clones; Fig. 3c). All the isoforms conformed to consensus splice donor and splice acceptor sites (“*gt*” and “*ag*” and their flanking sequences; Fig. 3a). Providing additional confirmation, TOPO cloning and sequencing of the RT-PCR products obtained from the IFN-treated human melanoma cells (see Fig. 2g) revealed the same LY6S isoforms to those observed in spleen.

Although belonging to the LY6/uPAR family of proteins, which normally contain 10 consensus cysteine residues, the LY6S-iso1 protein is special in that it contains a noncanonical serine residue in place of the sixth cysteine residue present in all other LY6-like proteins, hence the “S” in the LY6S designation. The serine codon was observed in cDNAs generated from both spleen and IFN-treated melanoma cells, and all genomic databases investigated show a codon at this position in the *LY6S* gene, in the genomic DNA, coding for a serine residue.

Because the LY6S gene and LY6S mRNAs described in this article are novel, it was important to find independent supportive evidence for their presence from freely available databases. Analyses of public domain human spleen RNA-seq data showed transcripts in the human spleen that are derived from the LY6S gene (Fig. 4, Supplemental Fig. 3), providing unambiguous validation for the existence of mRNAs coding for the LY6S-iso1 and LY6S-iso2 proteins.

LY6S is syntenic to eight murine Ly6 genes that form the Ly6a subfamily cluster of genes

In contrast with the sole human *LY6S* gene present in the region bordered by *LY6E* and *LY6L*, the syntenic mouse locus within which *Ly6a* resides contains eight Ly6 genes, all of which are highly similar to each other (Figs. 1a, 1e, 3d). These murine Ly6 genes demonstrate coordinated transcriptional responses to certain inflammatory cytokines and to those relating to IFN-mediated immune sensing (17, 18).

The eight Ly6 family genes are defined as belonging to the Ly6a subfamily (Figs. 1e, 3d). Both phylogenetic analyses (Fig. 1e) and protein similarity analyses (Fig. 3d) indicate that of all the mChr15-Ly6 proteins, the human LY6S-iso1 protein is most similar to the proteins encoded by the Ly6a subfamily. All the murine Ly6s-subfamily genes code for proteins with the amino acid sequence “ERAQGL” at the C-terminal regions of their SP, a sequence also conserved in the human LY6S protein (boxed red rectangles in Figs. 3, 5a), yet not present in any of the other hChr8 LY6 proteins.

The constructed phylogenetic maximum likelihood tree (Fig. 1e) shows *LY6S* branching at the base of the Ly6a subfamily clade containing the eight *Ly6* mouse genes located within the 500-kb subregion. A bootstrap value of 89% shows that the phylogenetic signal from the whole alignment lends strong support to this grouping. This tree supports the notion that *LY6S* has evolved from the same ancestral gene as the *Ly6a* subfamily clade, and that there have been several duplication events in the mouse. The similarity of *LY6S* to the eight *Ly6a* subfamily genes, as well as their syntenic colocalization (both flanked by *LY6E/Ly6e* and *LY6L/Ly6l*), indicates that the eight Ly6a subfamily genes are homologous to the solitary human *LY6S* gene, and this is a 1:8 orthology relationship (Figs. 1a, 1e, 3d). Comparison with other well-annotated vertebrate genomes suggests that the most parsimonious explanation is that there has been a gene expansion of *Ly6* genes in mouse, rather than one or more deletion events in other species.

A protein BLAST search with LY6S-iso1 yielded as the best hits the lymphocyte Ag Ly6a (Ly6A-2/Ly6E-1) proteins from *Nannospalax galili* (Upper Galilee Mountain blind mole rat), *Microcebus murinus* (gray mouse lemur), *Merionus unguiculatus* (Mongolian gerbil), and *Peromyscus maniculatus bairdii* (North American deer mouse) with e values of 1e-38, 3e-30, 2e-28, and 7e-28, respectively (see Fig. 5a for a comparison of LY6S-iso1 with the Nannospalax and Peromyscus Ly6a [Ly6A-2/Ly6E-1] proteins). Subsequent pairwise comparison of each human LY6 protein present on chromosome 8 with the deer mouse Ly6A-2/6E-1-like protein showed that LY6S gave the best match by far (Fig. 5c-e).

LY6-iso1 protein is expressed by IFN-treated cells and by spleen cells

To facilitate investigation into *LY6S* expression at the protein level, we generated LY6S-iso1-specific mAbs designated 5E12. The specificity of 5E12 was confirmed by the following results. First, 5E12 bound to recombinant hFc-LY6S fusion protein (Fig. 6b, lane 6), and binding was blocked by the immunizing LY6S peptide E and a peptide contained within this sequence (Fig. 6b, lanes 7 and 9, respectively; see Fig. 6a for peptide sequences within the LY6S-iso1 protein), but not by peptide C, which is upstream of the immunizing peptide (Fig. 6b, lane 8). Second, 5E12 bound to a protein expected for the size of the LY6S-iso1 protein in Western blot analyses of HK293 cells infected with lentiviruses coding for the LY6S-iso1 protein (Fig. 6c, left panel, lanes 1 and 2), but not from cells infected with control lentiviruses (Fig. 6c, left panel, lane 3). Furthermore, LY6S-iso1 protein observed in cells infected with retroviral particles coding for the native LY6S-iso1 protein migrated slightly faster than the corresponding LY6S protein that contained a Flag-epitope at its N terminus, conforming to their difference in molecular mass (compare in Fig. 6c, lane 1 [with the Flag epitope] and lane 2 [LY6S protein without the Flag epitope]). Third, by flow cytometry, 5E12 detected cell-surface LY6S-iso1 protein, albeit at low levels, on intact HK293 cells infected with retroviral particles coding for LY6S-iso1, as expected for a GPI-linked protein (Fig. 6dii, 6diii). Fourth, anti-LY6S mAb 5E12 immunofluorescent analysis of HK cells transiently transfected with plasmids coding for the LY6S protein showed positively staining cells (Fig. 6eii, 6eiii), which were not seen with cells transfected with control empty plasmid (Fig. 6ei). The reproducible detection of expression at the cell surface at low levels (Fig. 6dii, 6diii) suggests that cells do not readily express the LY6S protein at the cell surface (and see later).

Human M12 melanoma cells treated with IL1- β (Fig. 6fi'), as well as with IFN- γ and IL-6 (Fig. 6fi'', i'''), demonstrated cell-surface LY6S protein expression. Similarly, U87 glioma cells treated with IFN- β showed cell-surface LY6S protein (Fig. 6fii'), as did cells treated with IL1- β (Fig. 6fii''). Thus, cytokine treatment of cells reproducibly induces the expression of cell-surface LY6S in both M12 melanoma and U87 glioma cells. Such expression is not detected in the absence of cytokine treatment (Fig. 6fi, 6fii).

Immunofluorescent staining of human spleen tissue showed a discrete subpopulation of LY6S-iso1-positive cells that accounted for ~5% of all spleen cells (Fig. 6gi). The immunizing peptide E abrogated staining (Fig. 6giii) confirming Ab specificity, whereas peptide C, which was not used for immunization (Fig. 6gii), had no effect. LY6S-iso1 localized to the cell surface (Fig. 6giv') but was also observed within the cell (Fig. 6giv). LY6S-iso1 protein expression was barely detectable in other lymphoid tissues, such as thymus and tonsils, as assessed by immunohistochemical staining (Fig. 6hii, 6hiii), yet was seen clearly in spleen cells (Fig. 6hi) stained under identical conditions. Spleen tissue costained for LY6S-iso1 together with Abs directed against additional cell-surface proteins that define particular cell types detected a prominent subpopulation of LY6S-positive cells constituting ~5% of all the human spleen cells (Figs. 6gi, 6hi, 7b', 7b'', 7e-o). Staining of thymus, tonsil, and spleen with anti-CD45, a pan-leukocyte marker (leukocyte common Ag), showed many CD45⁺ cells in all three lymphoid-rich tissues (Fig. 7a-c). Costaining with anti-LY6S Abs revealed that only the spleen contained LY6S-positive cells (Fig. 7b'), distinguishing it from the LY6S-negative thymic and tonsillar tissues (Fig. 7a', 7c'). Abs against CD8 (Fig. 7e), CD4 (Fig. 7f), CD34 (Fig. 7g), CD19 (Fig. 7h), CD11b (Fig. 7i), FoxP3 (Fig. 7j), CD11c (Fig. 7k), CD20 (Fig. 7l), CD117-cKit (Fig. 7m), CD68 (Fig. 7n), and CD31 (Fig. 7o) showed no colocalization of any of these markers with LY6S-iso1-positive cells, suggesting that the LY6S-positive cells do not belong to a classical lineage of lymphoid cells. In contrast with the other tested leukocyte markers, a discrete subpopulation representing ~10% of the LY6S-positive splenic cells also expressed the leukocyte common Ag marker CD45 (Fig. 7b'', 7d), indicating that a subset of LY6S-iso1⁺ and CD45⁺ cells express both proteins.

Expression of the LY6-iso1 protein elicits changes in cell growth

That LY6S expression was observed only after cytokine treatment of cells (Figs. 2f, 2g, 2j, 6f, 6fi') suggested that LY6S expression may be related to an activated cell phenotype. To test this supposition, we infected human cell lines with retroviral particles coding for the GPI-linked cell-surface LY6S-iso1 protein or for the secreted LY6S-iso2 protein. Cells expressing the secreted LY6S-iso2 protein showed no differences in gross morphology compared with control cells stably infected with control pQCXIP plasmid (Fig. 8ai, compare right inset [LY6-iso2] with left inset [control vector]). However, cells infected with particles coding for the cell-surface-linked LY6S-iso1 protein showed changes in cell morphology (compare cells expressing LY6-iso1 in Fig. 8aii, 8aii', 8bii, 8bii', 8cii, 8cii' with cells expressing control vector in Fig. 8ai, 8ai', 8bi, 8bi', 8ci, 8ci'), where cells expressing LY6S-iso1 protein were large and many contained prominent cytoplasmic vacuoles (see, e.g., Fig. 8aii'). Cells displaying this phenotype included U87 (glioma; Fig. 8aii, 8aii'), MCF7 (breast carcinoma; Fig. 8bii, 8bii'), and YDFR (melanoma; Fig. 8cii, 8cii'). The

LY6S-iso1–expressing puromycin-resistant cells initially grew slowly (as shown for YDFR melanoma cells expressing LY6S-iso1; Fig. 8d). However, after three to four passages, the LY6S-iso1 cells resumed growth, reached plate confluency, and could then be subcultured (Fig. 8e).

Cells expressing the LY6S-iso1 protein have increased resistance to viral infection

Because transcription of the *LY6S* gene is IFN inducible and LY6S-iso1 expression is associated with changes in cell morphology and growth, we investigated whether LY6S-iso1 protein expression impacts cell resistance to viral infection. In all three human cell lines investigated, M12, YDFR, and U87, LY6S-iso1 protein expression was associated with a marked diminishment in VSV viral replication (Fig. 9). In M12 melanoma cells, LY6-iso1 expression led to a decrease in viral yield that exceeded two orders of magnitude (Fig. 9c, 9d), and a marked decline of viral yields was also seen in human YDFR melanoma and human U87 glioblastoma cells that express the LY6-iso1 protein (Fig. 9a, 9b, 9d).

Expression of the LY6-iso1 protein elicits an inflammatory cell phenotype

The changes observed in the phenotype of LY6S-iso1–expressing cells suggested an altered gene expression profile. To test for this, we performed next generation sequencing (both Illumina single-read sequencing and PE True Stranded) on RNA isolated from triplicate U87 glioblastoma cell cultures infected with control pQCXIP plasmid (U87-control) or from cells stably expressing cell-surface-linked LY6S-iso1 protein (designated “U87-LY6S-iso1”). Genes coding for chemokines, chemokine receptors, cytokines, and other proteins associated with an inflammatory cell phenotype were markedly upregulated in the LY6S-iso1–expressing cells (Fig. 10a, 10b, shown as volcano and heatmap plots, respectively; see Supplemental Table II). These included the following: cytokines (IL-1A, IL-1B, IL-6, IL-11, IL-24, IL-36B, CD274 [PDL1], CSF2, CSF3, EREG, FGF2, GDNF, HBEGF, LIF, and TNFSF8), chemokines (CXCL1, CXCL2, CXCL3, CXCL5, CXCL8, CX3CL1, and CCL20), chemokine receptors (ACKR3, CMKLR1, and IL-36RN), genes directly related to inflammation and immune responses (BCL2A1, BGN, LCN2, LCP1, NFkB1, NLRP12, RCAN1, PTGS2, RGS16, and SDC3; downregulated: CXADR, DEPTOR, DKK1, HMOX1), and genes related to IFN and cytokine signaling (IRF5, NFKBIZ, and SOCS1; downregulated: ID1 and SNAI1). Ingenuity analyses (Qiagen IPA as detailed in Materials and Methods) of the RNA-seq data identified the following biological pathways with very high p values, canonical pathways [$-\log(p \text{ value})$], and annotations of “diseases and functions”(p value): (1) granulocyte adhesion and diapedesis [12.8], (2) role of cytokines in mediating communication between cells [9.86], (3) differential regulation of cytokine production in macrophages and Th cells by IL-17A and IL17-F [6.89], (4) role of pattern recognition receptors in recognition of bacteria and viruses [6.82], (5) acute inflammatory response (2.99E–13), (6) accumulation of myeloid cells (1.26E–17), (7) accumulation of leukocytes (6.75E–17), (8) cytokine- and chemokine-mediated signaling pathways (3.29E–16), and (9) accumulation and recruitment of granulocytes (2.2E–14) and phagocytes (1.76E–14). These pathways reflected the alterations in gene expression patterns elicited by LY6S-iso1 expression, particularly of genes coding for cytokines, chemokines, chemokine receptors, IFN, and immune- and inflammatory-related proteins (Fig. 10a, 10b).

These results were confirmed at the protein level with cytokine/chemokine arrays, which showed increased secretion by the LY6S-iso1-expressing U87 cells of CXCL1, IL-1ra, CSF2, IL-6, and MIP-1a (Fig. 10c, 10d).

That LY6S-iso1 elicits expression of genes associated with an inflammatory phenotype was substantiated in the additional human cell lines, M12 and YDFR. In each of the three cell lines investigated (M12, YDFR, and U87), LY6S-iso1 elicited increased expression (using the stringent criteria of adjusted $p < 0.05$, counts > 30 , and a fold change > 2) of IL-1B, CXCL8, LIF, PCDH1, ADAMTS4, and STC1, all genes associated with an inflammatory cell phenotype (Fig. 11). Less stringent criteria showed that in at least two of the three cell lines investigated, LY6S-iso1 elicited increased expression of the chemokines CXCL1, CXCL2, CXCL3, and CCL20 and of the ILs IL-6, IL-11, IL-12A, IL-23A, IL-33, and IL-36B (Fig. 11).

The following inflammation-associated genes were also upregulated in all three LY6S-iso1-expressing cell lines: NRG1 (7.7-, 42-, and 2.7-fold for M12, YDFR, and U87 cells, respectively), PTGS2 (1.6, 11, and 3.9), RCAN1 (1.5, 1.5, and 2.1), and SOCS1 (1.2, 1.9, and 2.8). For all three (LY6S-iso1-expressing) cell lines, the following canonical functional networks appeared in the top 14 pathways identified using the IPA (Supplemental Table II): dendritic cell maturation (2.236, 2.449, and 3.545, Z scores for M12, U87, and YDFR, respectively), IL-6 signaling (2, 1.89, and 2.121), acute-phase response signaling (2, 1.663, and 1.941), IL-8 signaling (2.236, 1.342, and 1.291), and neuroinflammation signaling (1.633, 1.342, and 1.512). The IPA-derived upstream regulator analysis provided further support for involvement of the LY6S-iso1 protein with an inflammatory cell phenotype. The list of upstream regulators (Supplemental Table II) included the following top Z -scoring upstream regulators for all three cell lines expressing LY6S-iso1: TNF (#1 in the list, with Z scores of 3.3, 5.0, and 5.3 for M12, U87, and YDFR cells, respectively), tetradecanoylphorbol acetate (#2; 3.6, 4.4, and 4.3), IL-1B (#3; 2.4, 5.1, and 3.6), LPS (#4; 2.9, 5.3, and 2.8), IL-17A (#5; 2.2, 4.7, and 4.0), NF- κ B (complex) (#7; 3.0, 4.4, and 2.9), ERK (#10; 3.1, 3.2, and 3.4), IKBKB (#12; 2.7, 4.1, and 2.6), IL-1A (#13; 3.2, 3.7, and 2.7), and IL-1 (#16; 3.2, 3.7, and 2.4). Additional upstream regulators included poly(rI:rC)-RNA (#20; 2.4, 3.8, and 2.9), TGF-B1 (#23; 2.4, 2.2, and 4.1), TLR3 (#25; 2.5, 3.6, and 2.5), and TLR9 (#26; 2.4, 3.8, and 2.5).

DISCUSSION

This study documents a previously unannotated human gene now designated *LY6S*. Analyses both at the RNA and protein levels, as well as TransMap and public domain RNA-seq data, provide evidence for the existence of the *LY6S* gene. At the RNA level, cloning and sequencing of the cDNA products generated by RT-PCR of human spleen samples showed mRNAs that code for three LY6S isoforms: LY6S-iso1 codes for a cell-surface protein, whereas LY6S-iso2 and LY6S-iso3 code for secreted proteins. LY6S-iso1 has the “fingerprint” features characteristic of the large LY6 protein family, including (1) spacing of cysteine residues, (2) exon/intron makeup, (3) the cysteine-cysteine doublet, followed by (4) the cysteine-asparagine doublet. What differentiates it from other LY6 family members is the consensus sixth cysteine residue replaced in LY6S-iso1 by a serine residue. We are

unaware of any other member of the LY6 protein family that shows this deviation from the LY6 consensus. Because the unpaired, nondisulfide cysteine residue is now free to form disulfide bonds with unbonded cysteine residues in other proteins, the odd number (9) of cysteine residues in LY6S-iso1 likely affects LY6S-iso1 protein interactions. Yet 9 of the 10 consensus LY6S cysteine residues are retained in the LY6-iso1 protein, indicating that the four disulfide bridges formed between the LY6 consensus cysteine (C) residues C#1 and C#5, C#2 and C#3, C#7 and C#8, and C#9 and C#10 (8) should all be intact. Snake toxins that contain eight cysteine residues, associated with four disulfide bridges, form the characteristic three-finger structure (7), as do the LY6 proteins that have five disulfide bridges (30). Furthermore, the N-terminal LU/uPAR domain of uPAR lacks a cysteine pair (31), yet still forms the LU/uPAR domain. It is reasonable to assume, therefore, that the LY6S-iso1 protein also adopts a TFP structure.

Although the data indicate that human *LY6S* is homologous to the Ly6a subfamily of LY6 genes, we do not know whether *LY6S* is the ortholog of a single gene of the murine Ly6a subfamily, or whether all eight murine genes and their protein products are an expansion of the solitary human *LY6S* gene. The phylogenetic analysis, as well as our additional similarity analyses, show that the eight murine Ly6 genes constitute a gene cluster, in which an ancestral gene likely underwent several duplication events, thereby forming the Ly6a subfamily cluster. Moreover, the TransMap algorithm of the UCSC (University of California, Santa Cruz) genome browser maps *Ly6a* to the human *LY6S* gene. These considerations led us to conclude that this is a one-to-many orthologous relationship, and *LY6S* is the human ortholog of the Ly6a subfamily genes.

Genes of the murine Ly6a subfamily play pivotal roles both in inflammation and in hematopoietic stem cells (e.g., Refs. 32–36), and many of the Ly6a subfamily genes are related both to an inflammatory cell phenotype and to IFN-related pathways (18, 19). Just like the genes of the Ly6a subfamily, it appears from our analyses that *LY6S* is also involved in inflammatory processes. RNA-seq analyses in three different human cell lines showed that expression of the LY6S-iso1 protein is associated with the expression of genes coding for chemokines, cytokines, and other proteins classically connected to an inflammatory cell phenotype. These findings lend further support, in addition to that provided by the phylogenetic and protein similarity analyses, to the notion that *LY6S* has a one-to-many orthologous relationship with the genes of the murine Ly6a subfamily gene cluster.

Like the genes of the Ly6a subfamily, the human *LY6S* gene is also an ISG. By inducing expression of hundreds of genes, IFNs and the protein products of the induced ISGs are critical players in the restriction of viral infections. In line with our findings that *LY6S* expression is both IFN inducible and associated with increased expression of genes related to inflammation and immune responses, we observed that LY6S-iso1 expression markedly inhibited viral replication, a phenomenon seen in each of the three different human cell lines investigated. This is likely indirectly mediated by LY6S-iso1, which, as noted earlier, leads to altered patterns of gene expression, which in turn affects virus replication. Thus, one of the functions of *LY6S* may be to elicit protection from viral infection, as already noted for *LY6E* (37).

LY6S expression at the RNA level was highest in spleen, whereas it was undetectable in bone marrow and peripheral blood leukocytes. At the protein level, immunostaining analyses identified the LY6S-iso1 protein in ~5% of all spleen cells, yet it could not be detected in classical lymphoid-rich tissues, such as thymus and tonsil. These findings suggest that the LY6S⁺ cells are likely not of a known classical hematopoietic or lymphoid cell lineage. In this respect, the expression pattern of *LY6S* in cells and tissues is different from that of murine *Ly6a*, which, in contrast with *LY6S*, is expressed in peripheral blood leukocytes, on lymphoid precursor cells and hematopoietic stem cells in the mouse bone marrow (38, 39), and in many CD4⁺ T cells in the spleen.

In line with the notion that LY6S expression does not designate a classical cell of the human myeloid lineage, immunofluorescent analysis for expression of CD11b, a prototypical marker of human macrophages and possibly for many cells of human myeloid lineages, failed to show significant colocalization in the spleen with LY6S-expressing cells, just as classical T and B cell markers also failed to colocalize with LY6S expression. However, ~10% of all CD45⁺ spleen cells, a pan-leukocyte marker, are also LY6S⁺ (see Fig. 7d), and very few CD11b⁺ cells, amounting to <1% of these cells, are also LY6S⁺. Certain subsets of spleen macrophages, such as red pulp, marginal zone, and marginal metallophilic macrophages, do not express high levels of CD11b, if at all, and because of this, the LY6S⁺ cells may belong to such a subset.

In an attempt to learn more about the LY6S-iso1⁺ spleen cells, we queried publicly available human spleen single-cell RNA-seq data, but because of their limited gene coverage and low sensitivity, LY6S-iso1⁺ cells could not be identified in the available single-cell RNA-seq datasets. Sorting of human spleen cells with the anti-LY6S-iso mAbs that we have generated into LY6S-iso1⁺ cells and LY6S-iso1⁻ cells, followed by RNA-seq analyses, might assist in the future identification of the [LY6S-iso1⁺] cell type.

In summary, to our knowledge, we have identified the new IFN-inducible human *LY6S* gene that is likely the long-sought human ortholog of genes belonging to the *Ly6a* subfamily. *LY6S* is expressed in a discrete subset of human spleen cells of a nonclassical lineage, and its expression is associated with an inflammatory cell phenotype and with the restriction of viral replication. Of particular therapeutic clinical interest are the recent findings showing that Ly6e and Ly6a serve as receptors for viral entry into the cell. Ly6e is a receptor for HIV (40), and Ly6a, expressed on the surface of murine brain endothelial cells, is the cell receptor for a recombinant adeno-associated virus (AAV-PHP.B), via which AAV-PHP.B can penetrate the blood-brain barrier and transduce gene cargo into the brain (41–45). Our findings indicate that human LY6S is the ortholog to the genes of the murine *Ly6a* subfamily, and as we have observed LY6S expression in human brain tissue, the discovery of *LY6S* as reported in this article may open up new possibilities for introducing therapeutic genes into the human brain. Furthermore, the LY6S proteins may serve as receptors for additional pathogenic viruses, thus leading to novel antiviral therapeutic strategies.

Supplementary Material

Refer to Web version on PubMed Central for supplementary material.

Acknowledgments

This work was supported by the Office of the Director General, Tel Aviv University (to D.H.W.) and Dr. Miriam and Sheldon G. Adelson Medical Research Foundation (Needham, MA; to I.P.W.).

Abbreviations used in this article:

hChr8	human chromosome 8
IPA	Ingenuity Pathway Analysis
ISG	IFN-stimulated gene
Ly6	lymphocyte Ag 6
mChr15	mouse chromosome 15
PE	Paired End
RNA-seq	RNA sequencing
SP	signal peptide
TFP	three-fingered protein
uPAR	urokinase-type plasminogen activator receptor
VSV	vesicular stomatitis virus

REFERENCES

- Levitin F, Weiss M, Hahn Y, Stern O, Papke RL, Matusik R, Nandana SR, Ziv R, Pichinuk E, Salame S, et al. 2008. PATE gene clusters code for multiple, secreted TFP/Ly-6/uPAR proteins that are expressed in reproductive and neuron-rich tissues and possess neuromodulatory activity. *J. Biol. Chem* 283: 16928–16939. [PubMed: 18387948]
- Galat A, Gross G, Drevet P, Sato A, and Ménez A. 2008. Conserved structural determinants in three-fingered protein domains. *FEBS J.* 275: 3207–3225. [PubMed: 18485004]
- Davies A, Simmons DL, Hale G, Harrison RA, Tighe H, Lachmann PJ, and Waldmann H. 1989. CD59, an LY-6-like protein expressed in human lymphoid cells, regulates the action of the complement membrane attack complex on homologous cells. *J. Exp. Med* 170: 637–654. [PubMed: 2475570]
- Meri S, Morgan BP, Davies A, Daniels RH, Olavesen MG, Waldmann H, and Lachmann PJ. 1990. Human protectin (CD59), an 18,000–20,000 MW complement lysis restricting factor, inhibits C5b-8 catalysed insertion of C9 into lipid bilayers. *Immunology* 71: 1–9. [PubMed: 1698710]
- Ploug M, Kjalke M, Rønne E, Weidle U, Høyer-Hansen G, and Danø K. 1993. Localization of the disulfide bonds in the NH₂-terminal domain of the cellular receptor for human urokinase-type plasminogen activator. A domain structure belonging to a novel superfamily of glycolipid-anchored membrane proteins. *J. Biol. Chem* 268: 17539–17546. [PubMed: 8394346]
- Beigneux AP, Gin P, Davies BS, Weinstein MM, Bensadoun A, Fong LG, and Young SG. 2009. Highly conserved cysteines within the Ly6 domain of GPIHBP1 are crucial for the binding of lipoprotein lipase. *J. Biol. Chem* 284: 30240–30247. [PubMed: 19726683]
- Tsetlin VI 2015. Three-finger snake neurotoxins and Ly6 proteins targeting nicotinic acetylcholine receptors: pharmacological tools and endogenous modulators. *Trends Pharmacol. Sci* 36: 109–123. [PubMed: 25528970]

8. Loughner CL, Bruford EA, McAndrews MS, Delp EE, Swamynathan S, and Swamynathan SK. 2016. Organization, evolution and functions of the human and mouse Ly6/uPAR family genes. *Hum. Genomics* 10: 10. [PubMed: 27098205]
9. Leth JM, Leth-Espensen KZ, Kristensen KK, Kumari A, Lund Winther AM, Young SG, and Ploug M. 2019. Evolution and medical significance of LU domain-containing proteins. *Int. J. Mol. Sci* 20: 2760.
10. Upadhyay G 2019. Emerging role of lymphocyte antigen-6 family of genes in cancer and immune cells. *Front. Immunol* 10: 819. [PubMed: 31068932]
11. Holmes C, and Stanford WL. 2007. Concise review: stem cell antigen-1: expression, function, and enigma. *Stem Cells* 25: 1339–1347. [PubMed: 17379763]
12. Billiau AD, Fevery S, Rutgeerts O, Landuyt W, and Waer M. 2003. Transient expansion of Mac1+Ly6-G+Ly6-C+ early myeloid cells with suppressor activity in spleens of murine radiation marrow chimeras: possible implications for the graft-versus-host and graft-versus-leukemia reactivity of donor lymphocyte infusions. *Blood* 102: 740–748. [PubMed: 12676788]
13. Rasmussen JW, Tam JW, Okan NA, Mena P, Furie MB, Thanassi DG, Benach JL, and van der Velden AW. 2012. Phenotypic, morphological, and functional heterogeneity of splenic immature myeloid cells in the host response to tularemia. *Infect. Immun* 80: 2371–2381. [PubMed: 22526678]
14. Zhan X, Fang Y, Hu S, Wu Y, Yang K, Liao C, Zhang Y, Huang X, and Wu M. 2015. IFN- γ differentially regulates subsets of Gr-1(+)CD11b(+) myeloid cells in chronic inflammation. *Mol. Immunol* 66: 451–462. [PubMed: 26021804]
15. Mosser DM, and Edwards JP. 2008. Exploring the full spectrum of macrophage activation. [Published erratum appears in 2010 *Nat. Rev. Immunol.* 10: 460.] *Nat. Rev. Immunol* 8: 958–969. [PubMed: 19029990]
16. Yona S, and Jung S. 2010. Monocytes: subsets, origins, fates and functions. *Curr. Opin. Hematol* 17: 53–59. [PubMed: 19770654]
17. Liddicoat BJ, Chalk AM, and Walkley CR. 2016. ADAR1, inosine and the immune sensing system: distinguishing self from nonself. *Wiley Interdiscip. Rev. RNA* 7: 157–172. [PubMed: 26692549]
18. Flanagan K, Modrusan Z, Cornelius J, Chavali A, Kasman I, Komuves L, Mo L, and Diehl L. 2008. Intestinal epithelial cell upregulation of LY6 molecules during colitis results in enhanced chemokine secretion. *J. Immunol* 180: 3874–3881. [PubMed: 18322195]
19. Kosa P, Szabo R, Molinolo AA, and Bugge TH. 2012. Suppression of Tumorigenicity-14, encoding matriptase, is a critical suppressor of colitis and colitis-associated colon carcinogenesis. *Oncogene* 31: 3679–3695. [PubMed: 22139080]
20. Braschi B, Denny P, Gray K, Jones T, Seal R, Tweedie S, Yates B, and Bruford E. 2019. [Genenames.org](https://www.genenames.org/): the HGNC and VGNC resources in 2019. *Nucleic Acids Res.* 47(D1): D786–D792. [PubMed: 30304474]
21. Izraely S, Sagi-Assif O, Klein A, Meshel T, Ben-Menachem S, Zaritsky A, Ehrlich M, Prieto VG, Bar-Eli M, Pirker C, et al. 2015. The metastatic microenvironment: Claudin-1 suppresses the malignant phenotype of melanoma brain metastasis. *Int. J. Cancer* 136: 1296–1307. [PubMed: 25046141]
22. Darriba D, Taboada GL, Doallo R, and Posada D. 2011. ProfTest 3: fast selection of best-fit models of protein evolution. *Bioinformatics* 27: 1164–1165. [PubMed: 21335321]
23. Dobin A, Davis CA, Schlesinger F, Drenkow J, Zaleski C, Jha S, Batut P, Chaisson M, and Gingeras TR. 2013. STAR: ultrafast universal RNA-seq aligner. *Bioinformatics* 29: 15–21. [PubMed: 23104886]
24. Anders S, Pyl PT, and Huber W. 2015. HTSeq—a Python framework to work with high-throughput sequencing data. *Bioinformatics* 31: 166–169. [PubMed: 25260700]
25. Love MI, Huber W, and Anders S. 2014. Moderated estimation of fold change and dispersion for RNA-seq data with DESeq2. *Genome Biol.* 15: 550. [PubMed: 25516281]
26. Martin M 2011. Cutadapt removes adapter sequences from high-throughput sequencing reads. *EMBnet.Journal* 17: 1–10.

27. Krämer A, Green J, Pollard J Jr., and Tugendreich S. 2014. Causal analysis approaches in Ingenuity Pathway Analysis. *Bioinformatics* 30: 523–530. [PubMed: 24336805]
28. Stanke M, Diekhans M, Baertsch R, and Haussler D. 2008. Using native and syntenically mapped cDNA alignments to improve de novo gene finding. *Bioinformatics* 24: 637–644. [PubMed: 18218656]
29. Zhu J, Sanborn JZ, Diekhans M, Lowe CB, Pringle TH, and Haussler D. 2007. Comparative genomics search for losses of long-established genes on the human lineage. *PLOS Comput. Biol* 3: e247. [PubMed: 18085818]
30. Kieffer B, Driscoll PC, Campbell ID, Willis AC, van der Merwe PA, and Davis SJ. 1994. Three-dimensional solution structure of the extracellular region of the complement regulatory protein CD59, a new cell-surface protein domain related to snake venom neurotoxins. *Biochemistry* 33: 4471–4482. [PubMed: 7512825]
31. Ploug M, and Ellis V. 1994. Structure-function relationships in the receptor for urokinase-type plasminogen activator. Comparison to other members of the Ly-6 family and snake venom alpha-neurotoxins. *FEBS Lett.* 349: 163–168. [PubMed: 8050560]
32. Cook AD, Braine EL, and Hamilton JA. 2003. The phenotype of inflammatory macrophages is stimulus dependent: implications for the nature of the inflammatory response. *J. Immunol* 171: 4816–4823. [PubMed: 14568960]
33. Soudja SM, Ruiz AL, Marie JC, and Lauvau G. 2012. Inflammatory monocytes activate memory CD8(1) T and innate NK lymphocytes independent of cognate antigen during microbial pathogen invasion. *Immunity* 37: 549–562. [PubMed: 22940097]
34. Geng S, Chen K, Yuan R, Peng L, Maitra U, Diao N, Chen C, Zhang Y, Hu Y, Qi CF, et al. 2016. The persistence of low-grade inflammatory monocytes contributes to aggravated atherosclerosis. *Nat. Commun* 7: 13436. [PubMed: 27824038]
35. Askenase MH, Han SJ, Byrd AL, Morais da Fonseca D, Bouladoux N, Wilhelm C, Konkel JE, Hand TW, LacerdaQueiroz N, Su XZ, et al. 2015. Bone-marrow-resident NK cells prime monocytes for regulatory function during infection. *Immunity* 42: 1130–1142. [PubMed: 26070484]
36. Gao X, Cao Q, Cheng Y, Zhao D, Wang Z, Yang H, Wu Q, You L, Wang Y, Lin Y, et al. 2018. Chronic stress promotes colitis by disturbing the gut microbiota and triggering immune system response. [Published erratum appears in 2018 *Eur. J. Immunol.* 115: E4542.] *Proc. Natl. Acad. Sci. USA* 115: E2960–E2969. [PubMed: 29531080]
37. Pfaender S, Mar KB, Michailidis E, Kratzel A, Boys IN, V'kovski P, Fan W, Kelly JN, Hirt D, Ebert N, et al. 2020. LY6E impairs coronavirus fusion and confers immune control of viral disease. *Nat. Microbiol* 5: 1330–1339. [PubMed: 32704094]
38. Morrison SJ, Wandycz AM, Hemmati HD, Wright DE, and Weissman IL. 1997. Identification of a lineage of multipotent hematopoietic progenitors. *Development* 124: 1929–1939. [PubMed: 9169840]
39. Kondo M, Weissman IL, and Akashi K. 1997. Identification of clonogenic common lymphoid progenitors in mouse bone marrow. *Cell* 91: 661–672. [PubMed: 9393859]
40. Yu J, Liang C, and Liu SL. 2017. Interferon-inducible LY6E protein promotes HIV-1 infection. *J. Biol. Chem* 292: 4674–4685. [PubMed: 28130445]
41. Deverman BE, Pravdo PL, Simpson BP, Kumar SR, Chan KY, Banerjee A, Wu WL, Yang B, Huber N, Pasca SP, and Gradinaru V. 2016. Cre-dependent selection yields AAV variants for widespread gene transfer to the adult brain. *Nat. Biotechnol* 34: 204–209. [PubMed: 26829320]
42. Batista AR, King OD, Reardon CP, Davis C, Shankaracharya, Philip V, Gray-Edwards H, Aronin N, Lutz C, Landers J, and Sena-Esteves M. 2020. Ly6a differential expression in blood-brain barrier is responsible for strain specific central nervous system transduction profile of AAV-PHP.B. *Hum. Gene Ther* 31: 90–102. [PubMed: 31696742]
43. Hordeaux J, Yuan Y, Clark PM, Wang Q, Martino RA, Sims JJ, Bell P, Raymond A, Stanford WL, and Wilson JM. 2019. The GPI-linked protein LY6A drives AAV-PHP.B transport across the blood-Brain barrier. *Mol. Ther* 27: 912–921. [PubMed: 30819613]

44. Huang Q, Chan KY, Tobey IG, Chan YA, Poterba T, Boutros CL, Balazs AB, Daneman R, Bloom JM, Seed C, and Deverman BE. 2019. Delivering genes across the blood-brain barrier: LY6A, a novel cellular receptor for AAV-PHP.B capsids. *PLoS One* 14: e0225206. [PubMed: 31725765]
45. Hordeaux J, Wang Q, Katz N, Buza EL, Bell P, and Wilson JM. 2018. The neurotropic properties of AAV-PHP.B are limited to C57BL/6J mice. *Mol. Ther* 26: 664–668. [PubMed: 29428298]

Author Manuscript

Author Manuscript

Author Manuscript

Author Manuscript

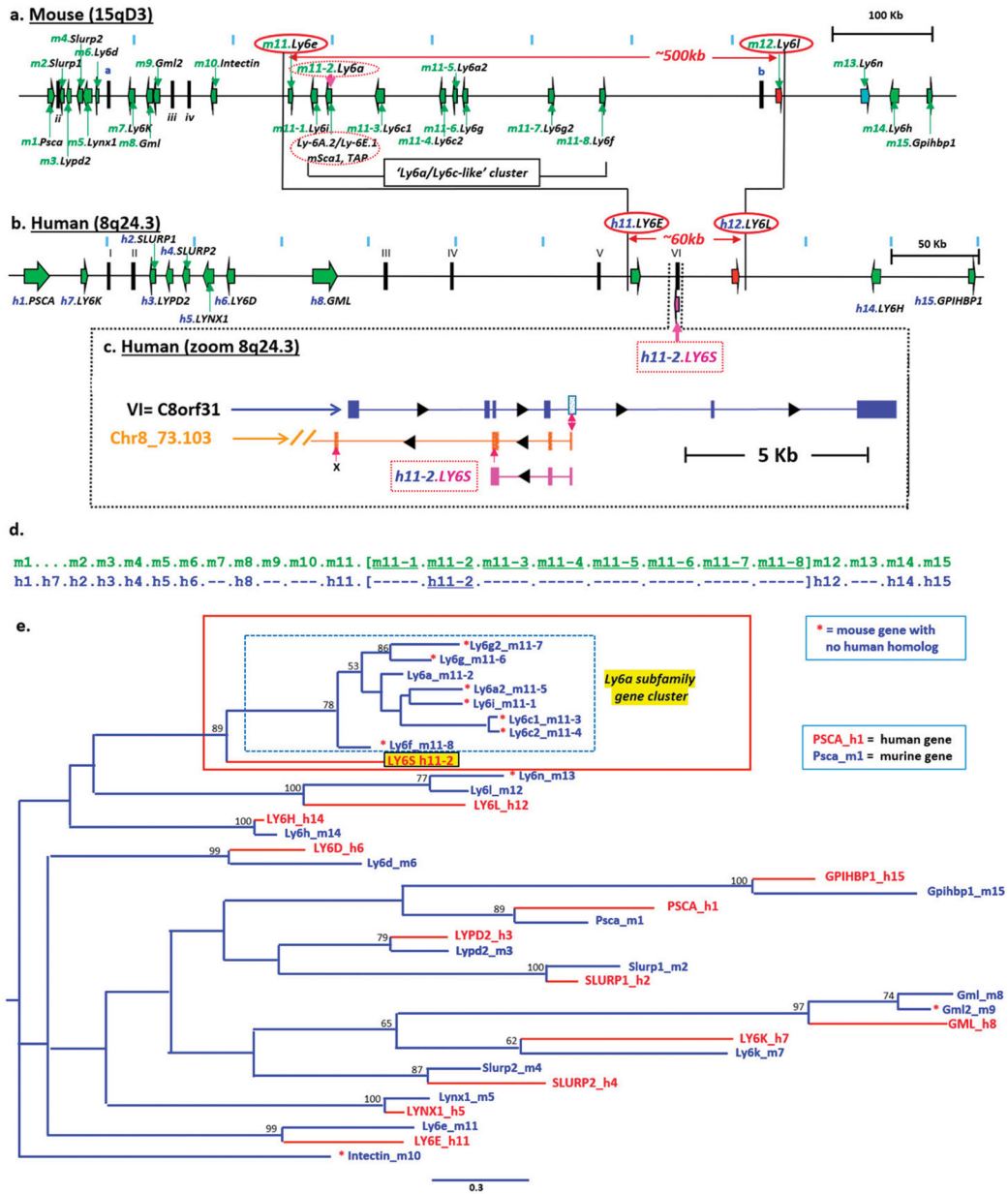


FIGURE 1. Ly6/LY6 loci in mouse chr15qD3 and human chr8q24.3, location of human LY6S, and phylogenetic tree of these Ly6/LY6 genes.

All known *Ly6/LY6* genes located on murine chr15qD3 and human chr8q24.3 are shown as green arrows with transcriptional orientation as indicated (a and b, respectively). Non-Ly6/LY6 genes appear as vertical black bars and are marked by small and capital Roman numerals (mouse and human, respectively). The murine *Ly6* genes are indicated as m1 through m15 and the eight murine *Ly6a* subfamily genes are indicated by m11–1 through m11–8; corresponding human genes have the prefix “h”; *LY6S* is designated h11–2 (a, b, and d). The murine *Ly6e* and *Ly6l* genes and the corresponding human *LY6E* and *LY6L* orthologs are encircled by red ovals (a and b). A zoom-in of the GenScan predicted gene (in orange) is shown in (c). (d) Schematic comparison of the murine (m1–m15) and corresponding human (h) genes. Dashes indicate no known human homolog. (e) Maximum

likelihood phylogenetic tree. Murine and human *Ly6/LY6* genes are indicated by blue and red fonts, respectively. Murine genes belonging to the Ly6a subfamily are bordered by the dashed blue outlined rectangle, and the human *LY6S* gene is shown in red fonts against a yellow background. Bootstrap support values >50% are shown above the nodes, branch lengths represent the expected number of substitutions per site, and the tree is shown as unrooted. The red asterisks indicate mouse genes with no previously identified human ortholog.

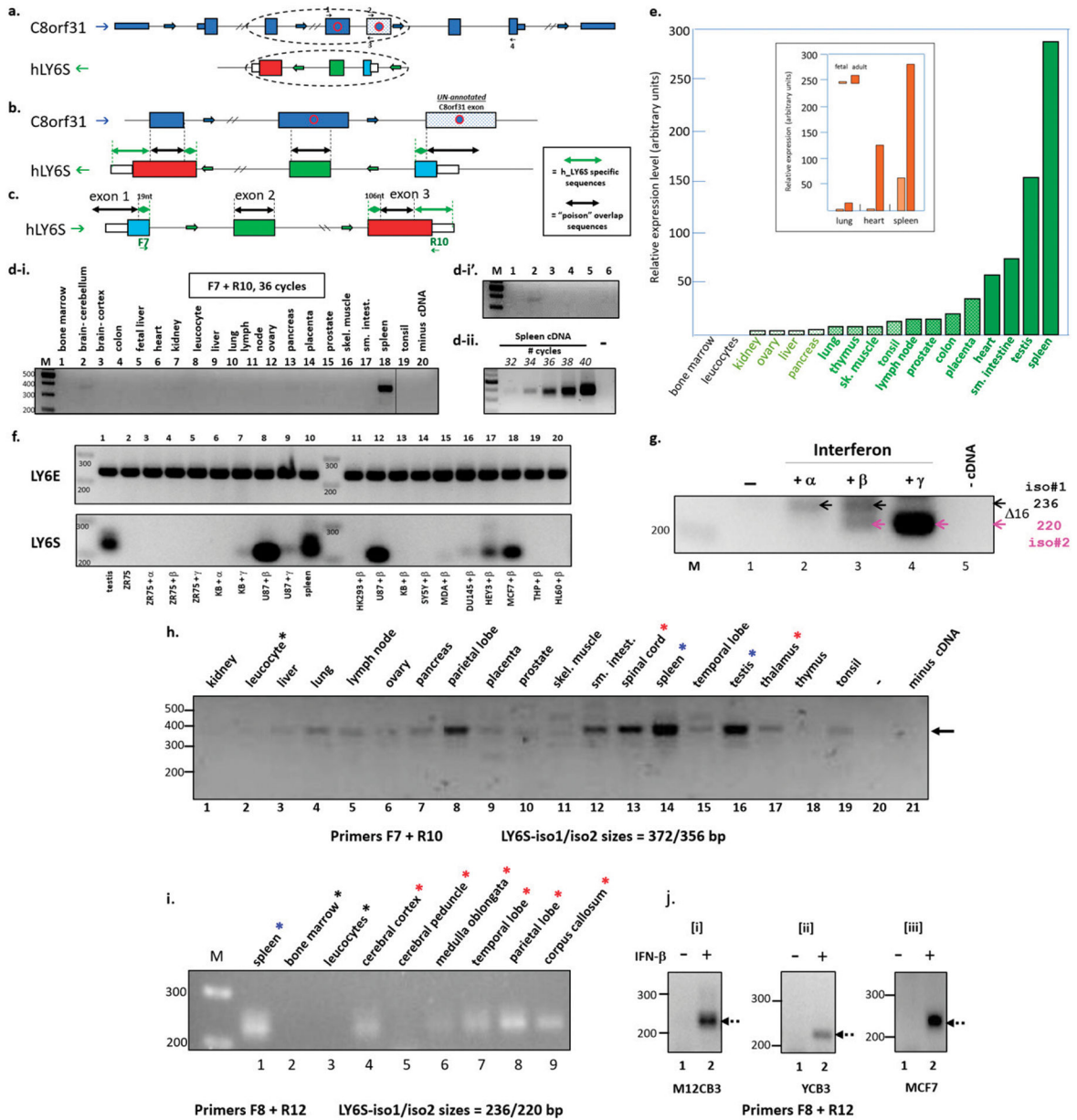


FIGURE 2. Exon overlap of the transcriptional units of LY6S and C8orf31; expression of LY6S mRNA in the human spleen, brain, and other tissues; and induction of LY6S mRNA expression by IFNs.

(a and b) *C8orf31* transcription proceeds left to right (blue arrows); *LY6S* is transcribed from the opposite strand, right to left (green arrows). An unannotated *C8orf31* exon is indicated by the stippled light blue box. Overlapping sequences are designated “poison” (black double-sided arrows), whereas regions specific for *LY6S* are marked by green double-sided arrows. (c) Transcription of *LY6S* is shown from left to right, together with the *LY6S*-specific forward and reverse primers F7 and R10. (di, di’ and dii) RT-PCR analysis of cDNAs derived from human tissues (36 cycles). Higher contrast exposure of lanes 1–6 is shown in (di’) and for different numbers of PCR cycles with spleen cDNA (dii). (e) *LY6S* expression in various adult tissues was assessed by qPCR. The inset compares relative

LY6S expression levels in fetal and adult tissues. **(f)** *LY6E* and *LY6S* expression (upper and lower panels, respectively) in testis and spleen (lanes 1 and 10, respectively) and from various human cell lines treated with IFN, as indicated, were assessed by RT-PCR. **(g)** *LY6S* expression in melanoma (M12CB3) cells that were untreated or treated with IFN- α , IFN- β , or IFN- γ (lanes 1–4, respectively) was assessed by RT-PCR. **(h)** RT-PCR analysis of cDNAs derived from human tissues (40 cycles), done with LY6S primers F7 and R10 (see Supplemental Table I). The arrow to the right indicates the approximate position for the expected sizes of the LY6S RT-PCR products with these primers (372/356 bp for iso1 and iso2, respectively), and DNA marker sizes are shown at the left. Tissues from the CNS are indicated by red asterisks, spleen and testis by blue asterisks, and the negative leukocyte sample by the black asterisk. **(i)** RT-PCR of additional regions of the brain done with LY6S primers F8 and R12. The arrow at the right indicates the approximate positions for the LY6S RT-PCR products with these primers (236/220 bp for iso1 and iso2, respectively). **(j)** RT-PCR of cDNAs from melanoma cells M2CB3 and YCB3 (**ji** and **jii**, respectively) and from MCF7 cells (**jiii**) done with LY6S primers F8 and R12 (see Supplemental Table I). The cells were treated with IFN- β (lane 2) or not treated (lane 1), as indicated.

subfamily genes are bracketed in blue and indicated by blue asterisks. Identical amino acids appearing four or more times in the different Ly6/LY6 proteins are highlighted using a white bold font against a black background. The highly conserved amino acid sequence “ERAQGL” appearing in the SPs of both the murine Ly6a subfamily cluster proteins and in LY6S-iso1 is boxed by the red rectangle. The Ly6/LY6 consensus cysteine residues of the Ly6 proteins (numbered 1–10) are indicated by yellow highlighted red bold fonts. The unique LY6S-iso1 serine (S) residue (arrow and yellow “&” against a red background) is indicated by the red highlighted yellow bold “S” text. The mouse *Ly6e* and *Ly6l* genes bordering the Ly6a subfamily cluster are indicated by black asterisks against green and red backgrounds, respectively. Amino acid sequences deleted from the alignment are indicated by the red “&” symbol. Because of their divergence from other mChr15-Ly6 proteins, Gml, Gml2, Gpihbp1, and mD730001G18Rik = 87 were not included in this analysis.

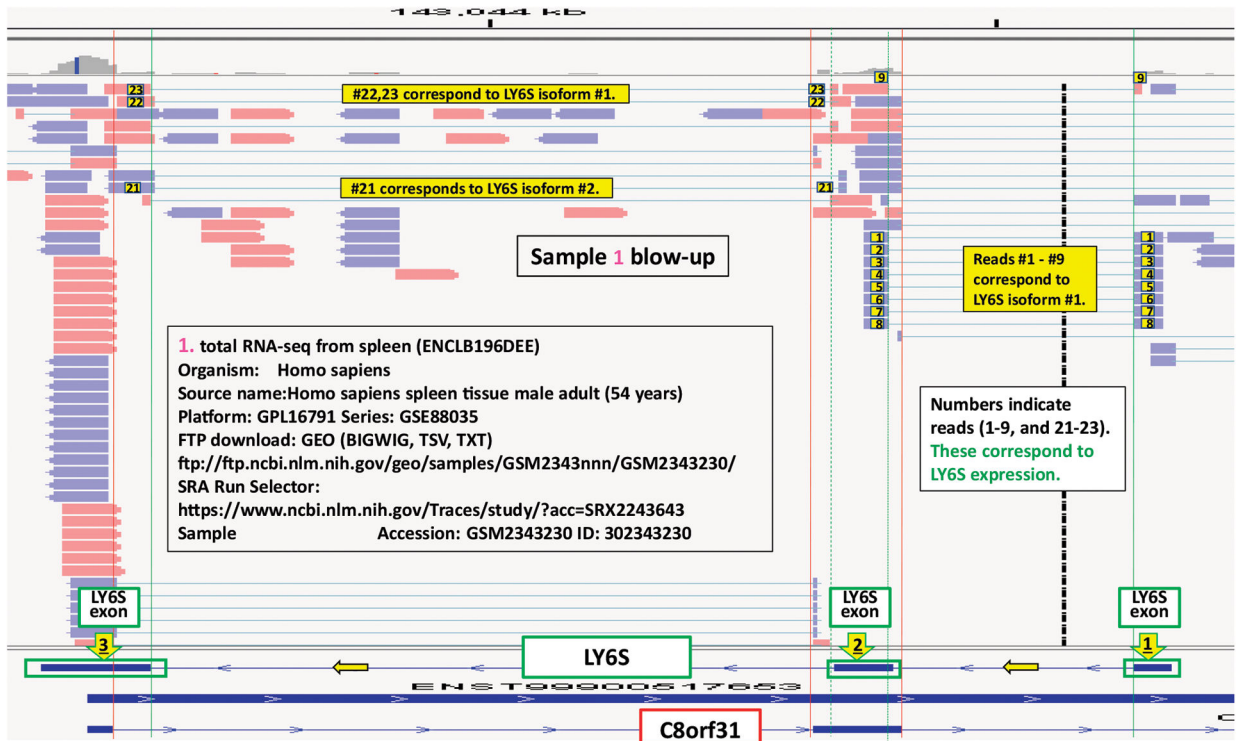


FIGURE 4. Analysis of human spleen total RNA-seq shows RNA reads that precisely correspond to transcripts derived from the LY6S gene.

The genomic coordinates of the human *LY6S* gene were introduced into our local gene database, and the RNA-seq data from human male spleen (GEO dataset ENCLB196DEE) were queried against this modified database. The reads mapping to the selected region of the *C8orf31* and (newly added) *LY6S* genes were analyzed, and transcripts deriving from *LY6S* are indicated (numbers in black bold fonts against a yellow background). The *LY6S* direction of transcription is indicated by the horizontal yellow arrows; the *LY6S* exons and *LY6S* splice junctions are shown by the downward-facing yellow arrows and vertical green lines, respectively. The vertical red lines show the *LY6S* splice sites. The detailed analyses of reads 1 and 22 are shown in Supplemental Fig. 3.

genes. The conserved “ERAQGL” sequence in the SPs of the Ly6a subfamily cluster of genes cluster proteins is indicated in bold blue fonts; identical amino acids appearing in both perLY6-Sca-1 and hLY6S are in bold red fonts in both sequences. Amino acid residues in other Chr8 LY6 proteins that are identical to perLy6a residues are in bold red fonts. The number of amino acid identities, as well as the percent identity with the reference PerLy6a sequence, is indicated (right).

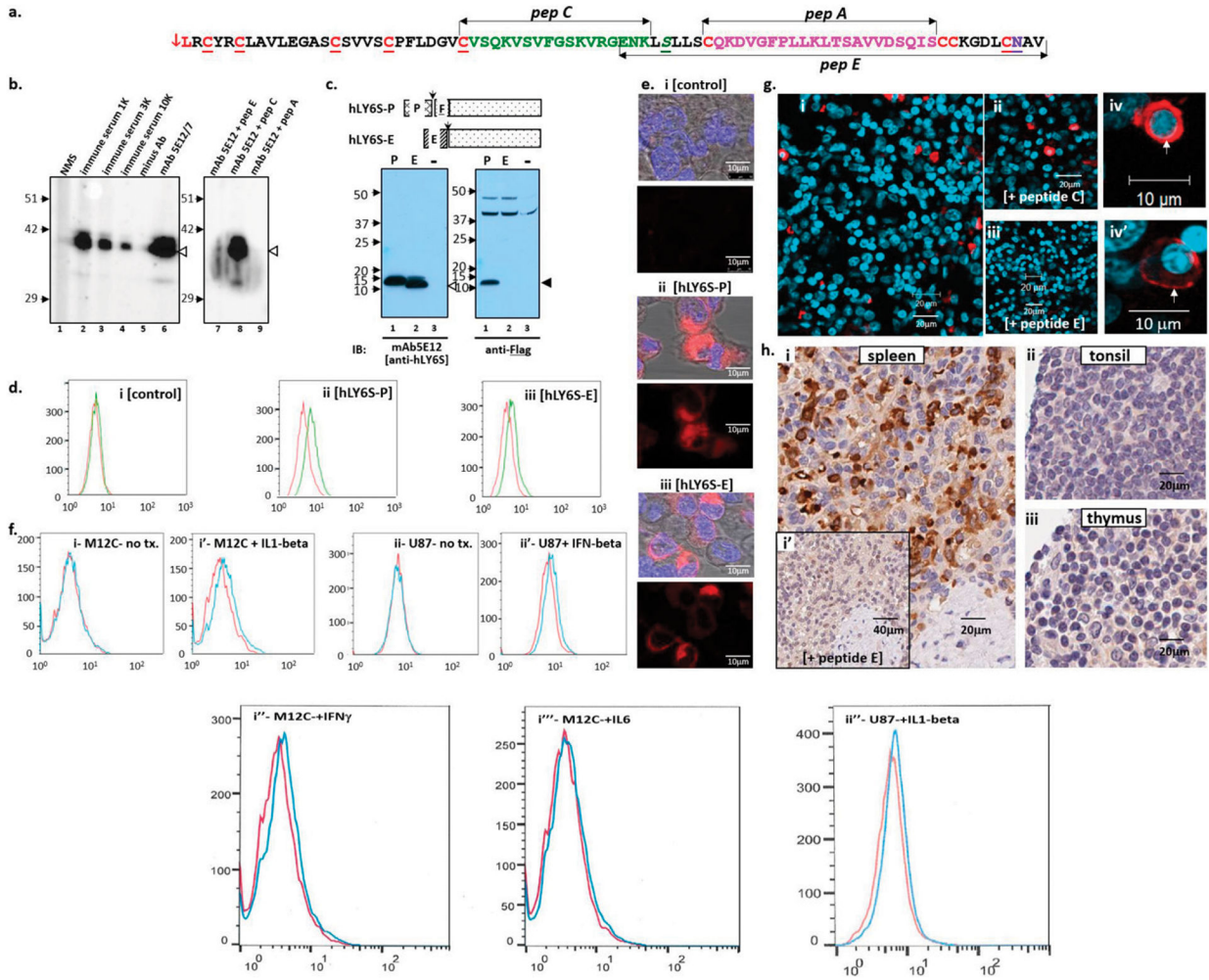


FIGURE 6. Detection of LY6S-iso1 in human spleen tissue and after treatment of cells with cytokines.

(a) Peptides A, C, and E, as indicated derived from the LY6S-iso1 protein, were synthesized, and mice were immunized with peptide E. (b) The anti-LY6S-iso1 polyclonal Abs (serum dilutions indicated) from a peptide E-immunized mouse or anti-LY6S-iso1 mAb-5E12 generated from the spleen of this mouse were used to probe an immunoblot of SDS-PAGE resolved hFc-LY6S-iso1 fusion protein (lanes 2–4 and 6, respectively); normal mouse serum served as control (lane 1). Similarly, an immunoblot of hFc-LY6S-iso1 protein was probed with anti-LY6S-iso1 mAb-5E12 in the presence of peptides E, C, and A (lanes 7–9, respectively). (c) Immunoblots of cell lysates prepared from HEK293 cell transfectants expressing either the native LY6S-iso1 protein (hLY6S-E, lanes indicated by “E”) or LY6S-iso1 protein in which the SP was replaced by the preprotrypsin SP followed by the Flag epitope (hLY6S-P, lanes indicated by “P”) were probed with mAb-5E12 (anti-LY6S-iso1) and with anti-Flag (left and right panels, respectively). Lysates from control cells are indicated by minus sign (–). (d) Nontransfected HEK293 cells and cells stably transfected with expression plasmids coding for LY6S-P or LY6S-E (di–diii, respectively) were analyzed by flow cytometry with anti-mouse secondary Ab alone (red lines) or with mAb-5E12 followed by fluorescently labeled secondary Abs (green lines).

(e) Nontransfected and HEK293 cells stably transfected with LY6S-P or LY6S-E (ei–eiii, respectively) were stained immunofluorescently with mAb5E12. (f) Human melanoma (M12C, fi, fi', fi'', fi''') or human glioblastoma (U87, fii, fii', fii'') cells were grown in the absence of cytokines (fi, fii) or with IL-1 β (fi'), IFN- γ (fi'', bottom of figure), IL-6 (fi''', bottom of figure), IFN- β (fii'), and IL-1 β (fii'', bottom of figure). The cells were assessed by flow cytometry as described for (d). (g) Sections of human spleen tissue were stained immunofluorescently with anti-LY6S-iso1 mAb-5E12 in the absence of peptides (gi), or in the presence of peptide C (gii) or peptide E (giii). LY6S-iso1⁺ spleen cells at higher magnification are shown in (giv) and (giv'). (h) Immunohistochemical staining of sections of human spleen, tonsil, and thymus with anti-LY6S-iso1 mAb-5E12 (hi–hiii, respectively) and of spleen with anti-LY6S-iso1 mAb-5E12 in the presence of competing peptide E (hi').

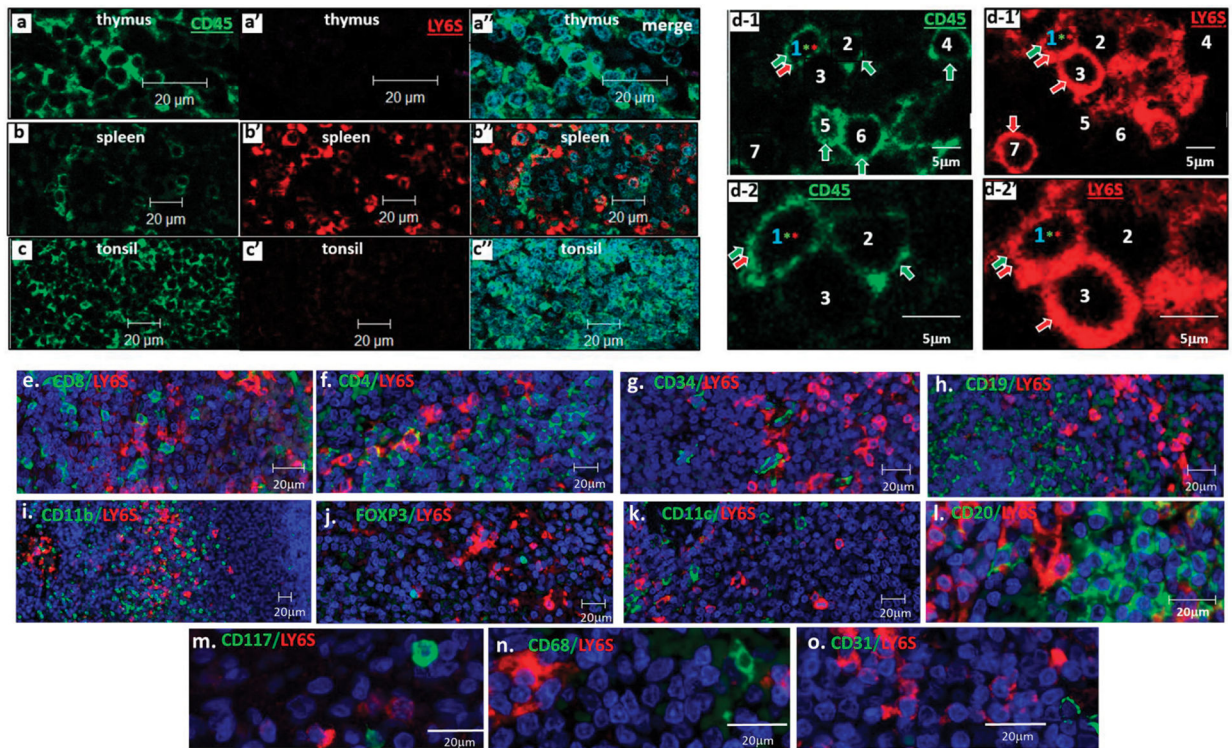


FIGURE 7. Immunofluorescent staining for the LY6S-iso1 protein and other cell-marker proteins in spleen, thymus, and tonsil.

(a–d) Sections of thymus, spleen, and tonsil were coimmunofluorescently stained for CD45 and LY6S-iso1 (green, a–c, and red panels, a'–c', respectively). Merging of the two stains is shown in (a''), (b''), and (c''). Different selected fields of spleen (d1, d1', d2, and d2') shown at two higher magnifications were stained immunofluorescently for CD45 (green, d1 and d2, green arrows) and for LY6S-iso1⁺ (red, d1' and d2', red arrows). The doubly positive CD45⁺/LY6S-iso1⁺ cell in this field is cell 1. (e–o) Spleen sections immunofluorescently stained for LY6S-iso1 (in red) and the indicated cell marker proteins (in bright green).

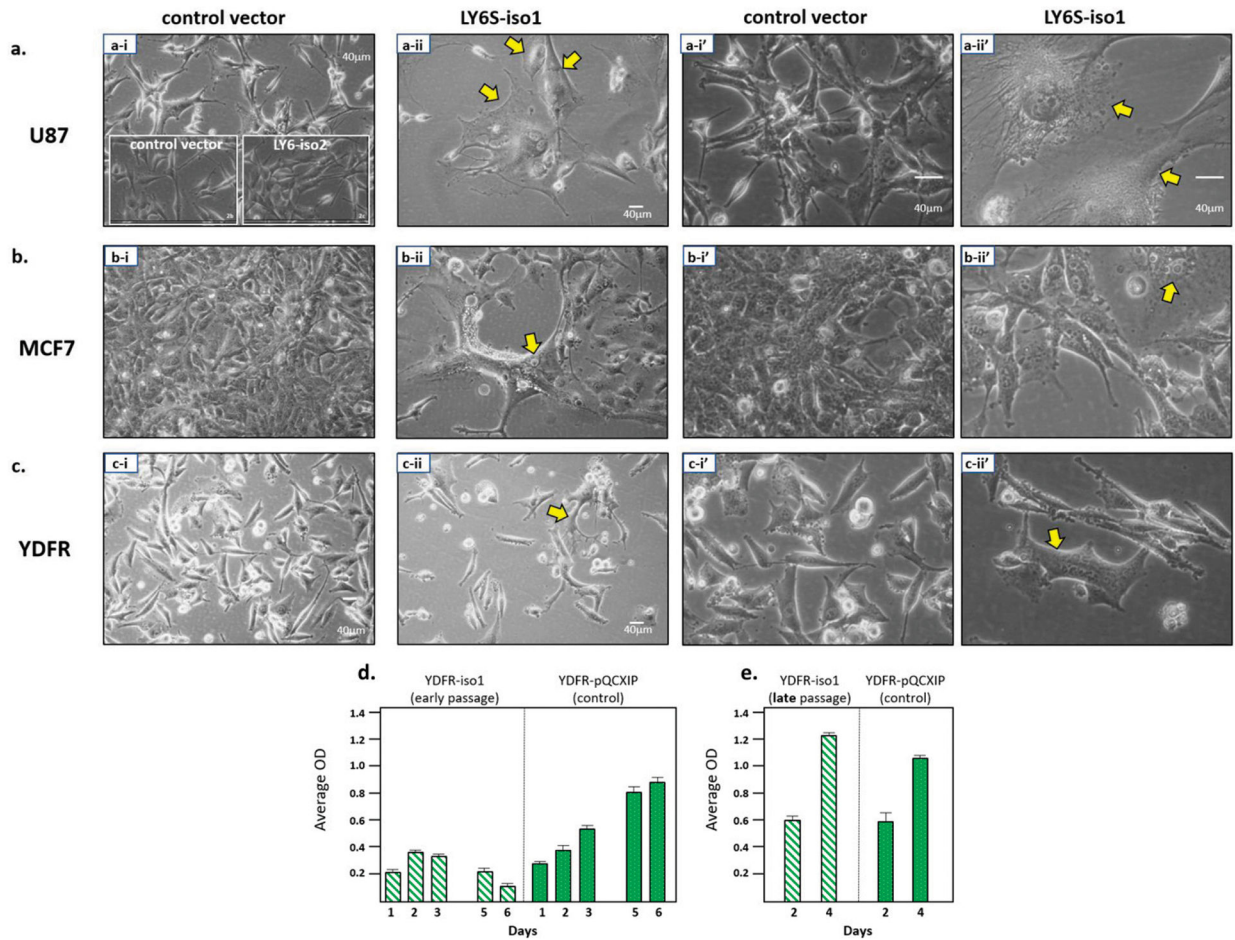


FIGURE 8. Cell morphology of human U87 glioblastoma, MCF7 breast carcinoma, and YDFR melanoma cells transfectants expressing LY6S proteins and growth of YDFR melanoma cells infected with LY6S-iso1.

U87, MCF7, and YDFR cells (a–c, respectively) stably transfected with pQCXIP-control vector (ai, bi, ci, and ai', bi', ci') or with pQCXIP coding for LY6S-iso1 protein (a-ii, b-ii, c-ii, and a-ii', b-ii', c-ii') were photomicrographed at low and high magnification (left and right sets, respectively). Exceptionally large cells with prominent vacuoles are indicated by yellow arrows. A comparison of control U87 cells with U87 cells expressing LY6-iso2 is shown in the insets in (ai). (d and e) YDFR melanoma cells stably infected with control pQCXIP plasmid (YDFR-pQCXIP) or YDFR cells expressing LY6S-iso1 taken at an early passage or late passage (YDFR-iso1 [early passage] and YDFR-iso1 [late passage]) were seeded in wells of a 96-well culture plate. Cell growth was monitored by the alkaline phosphatase assay.

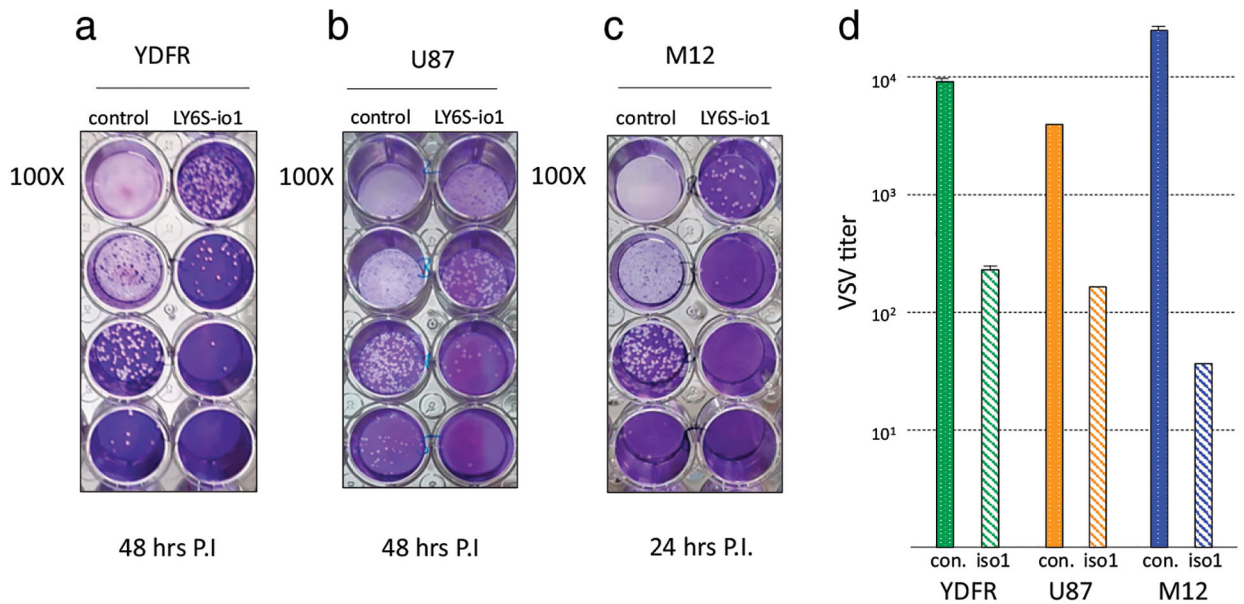


FIGURE 9. Inhibition of viral replication in cells expressing the LY6S-iso1 protein.

Human melanoma cells [YDFR-CB3 and M12-CB3, shown in (a) and (c)] or human glioblastoma cells [U87, shown in (b)] as indicated, were stably transfected with an empty expression vector (control) or with an expression vector coding for LY6S-iso1 (LY6S-iso1). VSV was added to the cell cultures, and virus present in the spent medium was assayed on monkey Vero cells, starting with a 100-fold dilution, followed by 10-fold dilutions. Quantitation of the viral titer in the spent medium of the virally infected cultures is shown in (d) (for YDFR cells, at 100-fold dilution, 48-h time point, and multiplicity of infection [MOI] of 0.05; for U87 cells, at 1,000-fold dilution, 48-h time point, and MOI of 0.015; and for M12 cells, at 100-fold dilution, 24-h time point, and MOI of 0.005). The number of viral plaques is indicated in square brackets above the bars for the respective cell types.

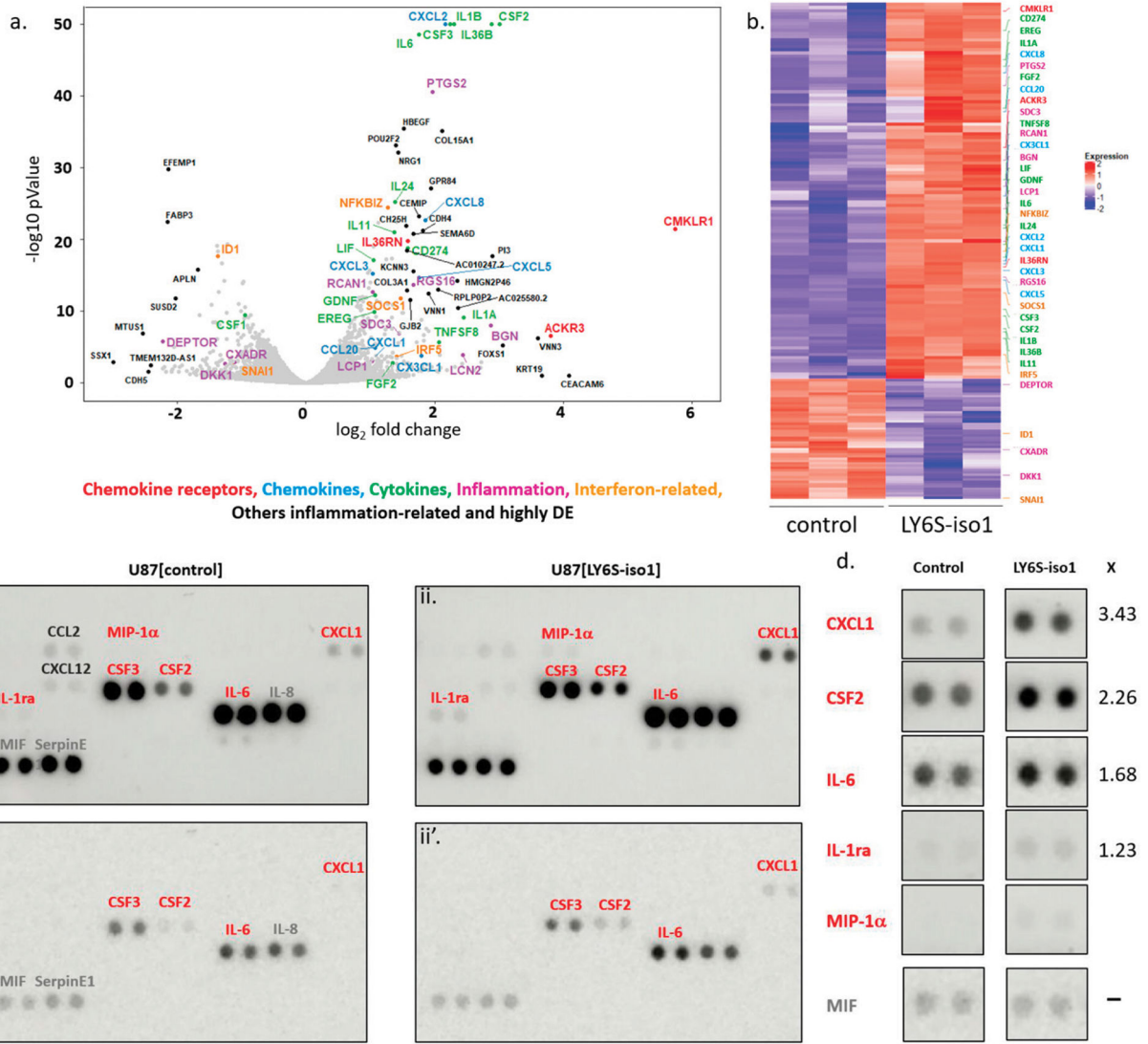


FIGURE 10. Volcano plot and heatmap of genes differentially expressed in LY6S-iso1-expressing U87 cells and profiling of selected secreted cytokines/chemokines.

(a and b) RNA extracted from triplicate cultures of puromycin-resistant U87 cells stably transfected with pQCXIP vector coding for LY6S-iso1 or with vector alone were subjected to RNA-seq analysis as described in the Materials and Methods, and the differential gene expression between the two groups is represented as a volcano plot (a) and as a heatmap (b). A selection of the differentially expressed genes was color coded as follows: chemokines, light blue; chemokine receptors, red; cytokines, green; inflammation, purple; IFN related, orange; others related to inflammation and also differentially expressed to a great extent, black. (c) Spent culture medium from U87 cells stably transfected with control pQCXIP plasmid (U87[control], ci and ci') or from U87 cells stably transfected with plasmid coding for LY6S-iso1 (U87[LY6S-iso1], cii and cii') were assayed for secreted cytokines and chemokines using a human cytokine/chemokine array. The probed arrays were exposed for either 10 min (ci and cii) or 10 s (ci' and cii'). Cytokines/chemokines increased in the LY6S-iso1-expressing cells are indicated in red fonts; cytokines/chemokines whose

expression remains unchanged are indicated by gray fonts (CCL2 and CXCL12 slightly downregulated in the LY6S-iso1-expressing cells are indicated with dark gray fonts). **(d)** Side-by-side comparisons of the chemokines/cytokines upregulated in U87[LY6S-iso1] cells using optimal exposure times. MIF provides an internal control for equal loading of spent medium from both cell types (lower two panels). Quantitation for the fold increase in the secreted cytokines was performed by ImageJ analyses.

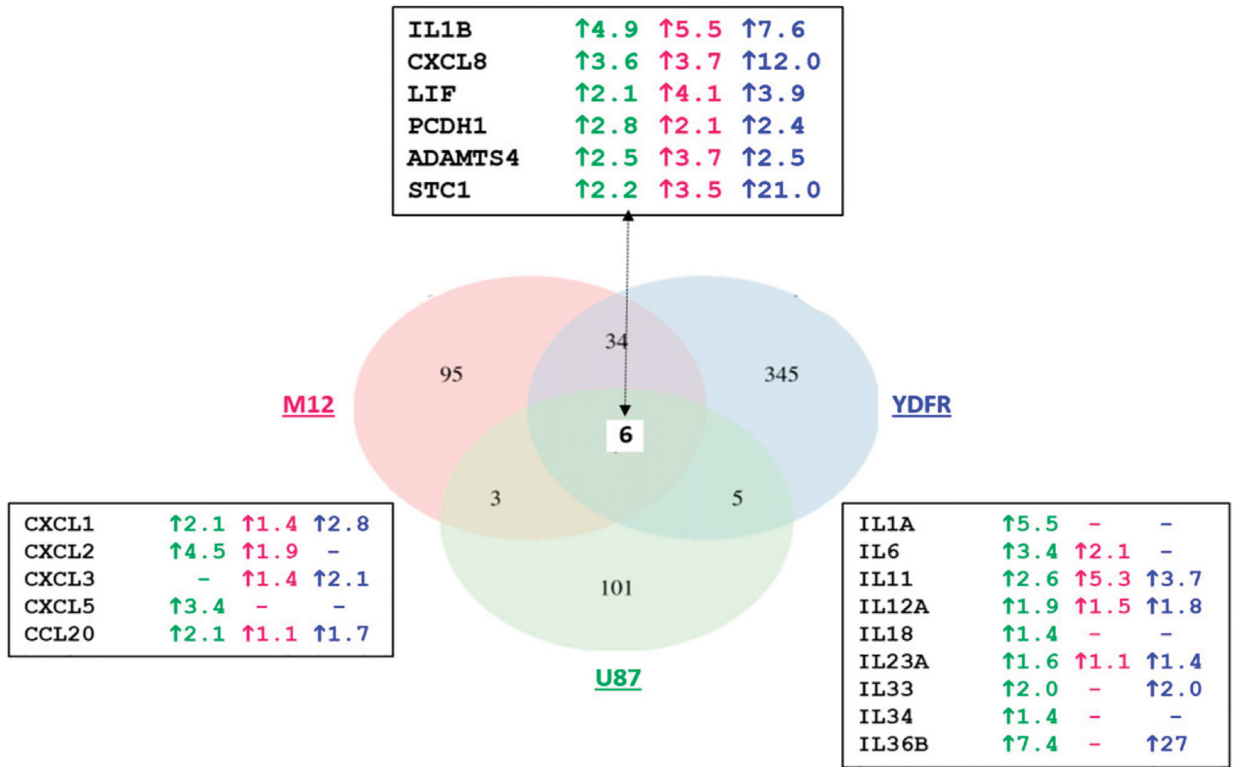


FIGURE 11. A comparison of the differentially expressed genes in the U87, M12, and YDFR cell lines that express the LY6S-iso1 protein.

The upregulated genes in the cells expressing the LY6S-iso1 protein as compared with their respective control non-LY6S-iso1-expressing cells are represented as a Venn diagram, using the stringent criteria of adjusted $p < 0.05$, maximum counts > 30 , and a fold change > 2 . The actual fold change for each cell line for the six genes that are upregulated in, and common to, all cell lines is shown in the top box (green, red, and blue fonts representing the U87, M12, and YDFR cells, respectively). The fold changes for certain chemokines (CXCL and CCL) and IL proteins are shown in the bottom left and bottom right boxes (dashes indicate no gene expression).